Astronomy & Astrophysics manuscript no. spitoni_MZR_MSR_accepted
August 4, 2020

On the connection between galactic downsizing and the most fundamental galactic scaling relations

E. Spitoni[1] ⋆, F. Calura[2], M. Mignoli[2], R. Gilli[2], V. Silva Aguirre[1], and A. Gallazzi[3]

[1] Stellar Astrophysics Centre, Department of Physics and Astronomy, Aarhus University, Ny Munkegade 120, DK-8000 Aarhus C, Denmark
[2] INAF-OAS, Osservatorio di Astrofisica e Scienza dello Spazio di Bologna, via Gobetti 93/3, I-40129 Bologna, Italy
[3] INAF – Osservatorio Astrofisico di Arcetri, Largo Enrico Fermi 5, I-50125 Firenze, Italy

Received xxxx / Accepted xxxx

ABSTRACT

Context. In their evolution, star-forming galaxies are known to follow scaling relations between some fundamental physical quantities, such as the mass-metallicity and the star formation main sequence relations.
Aims. We aim at studying the evolution of galaxies that, at a given redshift, lie simultaneously on the mass-metallicity and main sequence relations (MZR, MSR).
Methods. To this aim, we use the analytical, 'leaky-box' chemical evolution model of Spitoni et al. (2017b), in which galaxy evolution is described by infall timescale τ and wind efficiency λ. We provide a detailed analysis of the temporal evolution of their metallicity, stellar mass, mass weighted age and gas fraction.
Results. The evolution of the galaxies lying on the MZR and MSR at $z \sim 0.1$ suggests that the average infall time-scale in two different bins of stellar masses ($M_\star < 10^{10} M_\odot$ and $M_\star > 10^{10} M_\odot$) decreases with decreasing redshift through the addition of new galaxies with shorter timescales. This means that at each redshift, only the youngest galaxies can be assembled on the shortest timescales and still belong to the star-forming MSR. In the lowest mass bin, a decrease of the median τ is accompanied by an increase of the median λ value. This implies that systems which have formed at more recent times will need to eject a larger amount of mass to keep their metallicity at low values. Another important result is that galactic downsizing, as traced by the age-mass relation, is naturally recovered by imposing the local MZR and MSR for star-forming galaxies. This result is retained even assuming a constant star formation efficiency for different galactic masses (without imposing the observed scaling relation between stellar mass and gas depletion time-scales). Finally, we study the evolution of the hosts of C IV-selected AGN, which at $z \sim 2$ follow a flat MZR, as found by Mignoli et al. (2019). If we impose that these systems lie on the MSR, at lower redshifts we find an 'inverted' MZR, meaning that some additional processes must be at play in their evolution.
Conclusions. In our model, galactic downsizing is a direct consequence of the mass-metallicity and main sequence relations for star-forming galaxies. This poses a challenge for models of galaxy evolution within a cosmological framework.

Key words. galaxies: abundances - galaxies: evolution - galaxies: fundamental parameters - ISM: general

1. Introduction

In the last decades, several observational campaigns have confirmed that the evolution of star-forming galaxies is described by scaling relations between some fundamental physical quantities. For instance, a tight relation has been found between galactic stellar mass and metallicity (Lequeux et al. 1979; Maiolino & Mannucci 2019), the so-called mass-metallicity relation (hereinafter MZR). In the local Universe, the assessment of the MZR and other scaling relations was possible thanks to high-quality data collected within the Sloan Digital Sky Survey (SDSS), which have enabled to measure the flux ratios of the main optical emission lines for more than 100000 galaxies (e.g., Tremonti et al. 2004; Mannucci et al. 2010; Pérez-Montero et al. 2013; Lian et al. 2015).

Moreover, the observed evolution with redshift of the MZR (i.e. Maiolino et al. 2008; Yuan et al. 2013; Zahid et al. 2014) allows one to trace the chemical enrichment history of galaxies throughout different cosmic epochs. Zahid et al. (2014) pointed out that at redshifts $z < 1.6$, the MZR follows a steep slope with a 'knee' at a characteristic turnover mass at $M_* \sim 10^{10}\ M_\odot$. At stellar mass values higher than that, the MZR flattens as in the most massive galaxies metallicities begin to saturate. As a consequence, the redshift evolution of the MZR depends only on the evolution of the characteristic turnover mass. The evolving turnover mass can be related to the change in the gas-to-stellar mass ratio (see e.g. also the similar dependence between turnover mass and SFR in Curti et al. 2020).

Different theoretical scenarios have been presented in the past in order to explain the MZR, and they can be summarized as follows:

i) Galactic outflows: low-mass galaxies are more efficient in expelling metal-enriched matter than giant galaxies, because of the shallower gravitational potential wells of the former (Larson 1974; Tremonti et al. 2004; Spitoni et al. 2010, 2017b; Hirschmann et al. 2016). In the framework of pure chemical evolution models, a more recent work of Lian et al. (2018b) suggested that strong metal outflows occurring in the earliest galactic evolutionary phases also help reconciliating gas phase and the mass-weighted stellar MZRs.

⋆ email to: spitoni@phys.au.dk

ii) Variable star formation efficiency (SFE): the efficiency of star formation is larger in more massive systems, which have formed the bulk of their stars by means of an intense star formation event at high redshift, quickly enriching their ISM to solar or over-solar metallicities.
In the local universe, Boselli et al. (2014) presented a scaling relation between the typical galaxy gas depletion timescale and the galaxy stellar mass that can be easily transformed in SFE. They observed that massive galaxies consume the available gas reservoir on shorter typical timescales than dwarf galaxies. This means that larger galaxies are expected to experience, on average, higher SFEs (see also Matteucci 2012). Various chemical evolution studies support this scenario (Matteucci 1994; Lequeux et al. 1979; Calura et al. 2009).

iii) A third interpretation of the MZ relation is linked to the initial stellar mass function. (Köppen et al. 2007) showed how the MZ relation can be explained by a higher upper mass cut-off in the initial mass function (IMF) in more massive galaxies.

Chemical evolution models are powerful tools which help to probe fundamental processes regulating galaxy formation and evolution. They can provide important constraints on how subsequent stellar generations have modified the chemical composition of the interstellar medium (ISM), to give place to chemical abundance pattern as observed in present-day galaxies (Matteucci 2012). In this framework, Spitoni et al. (2017b) presented an analytical solution for the evolution of the galaxy metallicity, where an exponential infall of gas was assumed for the gas accretion rate, along with instantaneous mixing and instantaneous recycling approximation (IRA) (Matteucci 2012).

In their study of the MZR in the local SDSS star-forming galaxies by Peng et al. (2015), Spitoni et al. (2017b) found that lower mass galaxies suffered more intense winds compared to the higher mass ones, in agreement with the scenario i) mentioned above, and had to be characterized by shorter time-scales of gas accretion imposing the variable SFE by Boselli et al. (2014), as indicated by the scenario ii).

Another fundamental quantity to understand galaxy evolution is the star formation rate (SFR), which helps to shed light on the basic processes regulating the conversion of gas into stars and the growth of the stellar mass. The observations of large samples of star-forming galaxies in different redshift intervals have allowed to establish the existence of a well-defined relation between the SFR and the stellar mass, the so-called Main Sequence relation (MSR hereafter), thoroughly studied in several work (Brinchmann et al. 2004; Elbaz et al. 2007; Noeske et al. 2007; Peng et al. 2010; Santini et al. 2017; Pearson et al. 2018). As the MZR, also the MSR is characterized by a clear evolution with redshift. Pearson et al. (2018) studied the MSR in the redshift range between $z = 0.2 - 6$, showing that the slope of this relation does not change substantially with cosmic time. In particular, the slope of the MSR becomes steeper only for galaxies at high redshift, in the range between $3.8 \leq z \leq 6$. On the other hand, it has been ascertained in several studies that the zero point of the MSR increases with redshift (e. g., Santini et al. 2017, Iyer et al. 2018).

One of the most remarkable outcome of studies of scaling relations in local and distant galaxies was the discovery of substantial differences in the star formation history of low- and high-mass galaxies, also known as 'galaxy downsizing' (DS) (e.g. Cowie et al. 1996; Mortlock et al. 2011a). In the framework of galactic DS, the largest galaxies are assembled at the earliest times, with a large SFR values mostly concentrated in their earliest phases and accompanied by very efficient chemical enrichment (Calura et al. 2009; Matteucci 2012; Maiolino & Mannucci 2019). The phenomenology of Galactic downsizing is wide and multifaceted, as it is reflected by several observational aspects of galaxies at both low and high redshift, including color distributions at optical and infrared wavelegths of high-redshift galaxies (Cowie et al. 1996), studies of the integrated abundance rations in local early type galaxies (e. g., Spolaor et al. 2010 and references therein), studies of the evolution of the galactic stellar mass function (e. g., Mortlock et al. 2011b) and studies of metallicity, age and stellar mass from optical spectra of local galaxies (Gallazzi et al. 2005)

Altogether, these independent pieces provide the same indications, i. e. a more intense star formation activity in the most massive galaxies at early epochs, followed by higher star formation in low-mass galaxies at lower redshifts.

By means of an analytic chemical evolution model of Spitoni et al. (2017b), our aim is to study the the evolution of some basic properties of the galaxies which build the MZR and MSR at different redshifts. These properties include stellar mass and star formation activity, and how these are related to other quantities, such as the ages of the stellar populations. In performing this analysis, another aspect to be investigated is the connection between the fundamental scaling relations mentioned above (the MZR and MSR) and galactic DS.

We will also show the backward temporal evolution of the principal physical properties (i.e, gas fraction, metallicity, SFR, stellar mass) of star-forming galaxies that are part of the local MZR and MSR. Other studies investigated the backward evolution of the MZR in star-forming galaxies with chemical evolution models (Calura et al. 2009, Lian et al. 2018a), but without focus on the interplay with other scaling relations and on the particular role played by the MS.

We will also analyze the temporal evolution and the fate of the galaxies with stellar masses, metallicities and SFRs constrained by the high redshift MZRs and MSRs. In particular, we will discuss the implications of the newly observed, flat MZR at redshift $z = 2.2$ by Mignoli et al. (2019), who analyzed the metal content of 88 C IV-selected galaxies containing type 2 AGN with reliable measurements at high redshift.

Our paper is organized as follows. In Section 2, we recall the main features of the chemical evolution model of Spitoni et al. (2017b). In Section 3, the methodology used to create our grid of models is presented. In Section 4 we present the main observational constraints considered in this work and in Section 5 we present our main results assuming a Salpeter (1955) IMF. Our conclusions are drawn in Section 6.

2. The model by Spitoni et al. (2017b)

Spitoni et al. (2017b) presented new analytical solutions in presence of an infall of gas that follows an exponential law for the metal abundances, gas and stellar masses within a galactic evolutionary framework where instaneous mixing and IRA are assumed (Matteucci 2012). The infall of gas that follows an exponential law is a fundamental assumption adopted in most of the numerical chemical evolution models in which IRA is relaxed. Chemical evolution models of our Galaxy (Calura et al. 2009; Romano et al. 2010; Grisoni et al. 2018; Vincenzo et al. 2019; Spitoni et al. 2016, 2017a, 2019a,b, 2020) assume that the various different stellar components formed by means of separate accretion episodes of gas, with the accretion rate of each episode expressed by an exponential law.

In Spitoni et al. (2017b), the SFR is modelled by means of the Schmidt (1959) law, where the star formation rate $\psi(t)$ can be expressed as $\psi(t) = S \cdot M_{\rm gas}(t)$, and where $M_{\rm gas}(t)$ is the gas mass at the time t and S is the so-called star formation efficiency (SFE), which is commonly expressed in Gyr^{-1} and which is a free parameter of the model.

The gas infall rate is expressed by an exponential law $\mathcal{I}(t) = Ae^{-t/\tau}$, where τ is the infall time-scale. The quantity A is a constant, constrained by the total infall gas mass $M_{\rm inf}$ (Spitoni et al. 2017b).

In the model proposed by Spitoni et al. (2017b), gas outflows in galaxies have been taken into account as well. The outflow rate is proportional to the SFR in the galaxy (see Recchi et al. 2008; Spitoni et al. 2010; Spitoni 2015): $W(t) = \lambda \cdot \psi(t)$, with λ being the loading factor parameter (a dimensionless quantity).

2.1. The analytical solution

The analytical solution of Spitoni et al. (2017b) for the evolution of the gas-phase metallicity, defined as $Z = M_Z/M_{\rm gas}$, is:

$$Z(t) = \frac{y_z\, S(1-R)}{\alpha\tau - 1} \cdot \frac{M_{\rm gas}(0)\, t\, (\alpha\tau-1)^2 + A\tau[t - \tau(1+\alpha t) + \tau e^{\alpha t - t/\tau}]}{A\tau(e^{\alpha t - t/\tau} - 1) + M_{\rm gas}(0)(\alpha\tau - 1)}, \quad (1)$$

in which it is assumed that the infalling gas is metal-free, as is the the galaxy at the epoch of its formation. In Eq. (1) we introduce the parameter α, defined as $\alpha \equiv (1 + \lambda - R)S$. The quantities y_Z and R are the so-called yield per stellar generation and returned mass fraction (for a detailed description, see Spitoni et al. 2017b), respectively.

The values of y_Z and R are average values computed at various metallicities and for various IMFs, and are from Table 2 of Vincenzo et al. (2016), in which the compilation of stellar yields of Romano et al. (2010) was considered. As for the stellar IMF, two different cases are studied in this work. In the case of a Salpeter (1955) we assume $R = 0.287$ and $y_O = 0.018$, whereas for a Chabrier (2003) (see Appendix A) $R = 0.441$ and $y_O = 0.0407$, where y_O is the oxygen yield per stellar generation.

The other analytical expressions for the evolution of the total mass, gas mass and stellar mass can be found in Spitoni et al. (2017b).

More recently, Weinberg (2017) presented chemical analytical solutions adopting a different approach compared to Spitoni et al. (2017b), specifying the SFR history instead of an analytical form for the infalling gas. The SFR derived by an exponential infalling gas rate in Spitoni et al. (2017b) is similar to the linear-exponential SFR history (proportional to $te^{-t/\tau_{\rm sfh}}$, where $\tau_{\rm sfh}$ is the time-scale of the exponential decline) presented by Weinberg (2017), and the results for the metallicity evolution are qualitatively similar.

3. The methodology

We focus on a given redshift, and we impose that the galaxies must follow the observed MZR and the star-forming MSR measured at that redshift (see Section 4 for details concerning the observational constraints).

First, we study the properties of the local galaxies by imposing the MZR and the MSR at redshift $z = 0.1$, and analyzing their 'backward' evolution towards higher redshifts. On the other hand, by imposing the same scaling relations at higher redshift, we will compute a 'forward' evolution of the galaxies at lower redshifts and towards the present time.

In this framework, we will also study the evolution of the galaxies which at redshift $z = 2.2$ follow the flat MZR as derived by Mignoli et al. (2019).

A grid of galactic models is created by varying some key parameters within a wide, yet realistic space and with a fine resolution. The values adopted for the infall timescale τ span a range between 0.05 Gyr and 10 Gyr, with a resolution $\Delta\tau$=0.05 Gyr as in Spitoni et al. (2017b). The wind parameter λ can vary in the range between 0 and 10, with a resolution of $\Delta\lambda$=0.05, i. e. 10 times finer resolution than the one adopted in Spitoni et al. (2017b), where $\Delta\lambda$=0.5 . Moreover, as done in Spitoni et al. (2017b) the total infall mass in the Salpeter (1955) case varies between $10^{7.5}$ and $10^{11.5}$ M$_\odot$. In the case of the Salpeter (1955) IMF, we vary the infall masses accordingly to the following expression:

$$M_{inf} = (k/10) \cdot 10^{j+7.5}\ M_\odot, \quad (2)$$

where $1 \leq k \leq 100$, and steps $\Delta k = 5$, $1 \leq j \leq 3$ and steps $\Delta j = 1$. In the Appendix A, we will discuss the effects of a different IMF on this parameter. Each galaxy has been evolved in time with a resolution of Δt=0.036 Gyr.

Following Spitoni et al. (2017b), we do not assume that all galaxies are coeval, but we allow them to form at different redshifts. At a fixed stellar mass, a galaxy is considered as part of the local (or high-redshift) MZR and MSR if the differences between the predicted oxygen abundance and SFR values and the observed ones are smaller than 10^{-3}: i.e. Δ(O/H)=(O/H)$_{\rm model}$− (O/H)$_{\rm data}$ < 10^{-3} dex and Δlog(SFR) = log(SFR$_{\rm model}$) − log(SFR$_{\rm data}$) < 10^{-3} log(M$_\odot$ yr^{-1}). In this way we are assuming null scatter in the MZR and MSR.

Moreover, in order to be consistent with the observational data by Trussler et al. (2020), we define the average mass-weighted age following Calura et al. (2014). For each galaxy, characterised at a certain evolutionary time t by a SFR $\psi(t)$, we compute the average mass-weighted age at the time t_n as:

$$\mathrm{Age}(t_n) = \frac{\int_0^{t<t_n} (t_n - t)\psi(t)dt}{\int_0^{t<t_n} \psi(t)dt}. \quad (3)$$

Average mass-weighted ages have been computed at four different redshift values, each one corresponding to a different value for t_n. The star formation efficiency SFE is constrained by means of the scaling relation for local galaxies presented by Boselli et al. (2014) which link the typical galaxy gas depletion timescale, $\tau_{\rm gas}$, and the galaxy stellar mass as follows:

$$\log(\tau_{\rm gas}) = -0.73 \log(M_\star/M_\odot) + 16.75, \quad (4)$$

where $\tau_{\rm gas} = M_{\rm gas}/\mathrm{SFR}$ is defined as the inverse of our SFE, namely $\tau_{\rm gas} = 1/S$. According to Eq. (4), galaxies with higher stellar mass would consume their available gas mass on shorter typical timescales if only star formation activity were taking place in the galaxy; this means that larger galaxies are expected to experience, on average, higher SFEs (see Matteucci 2012).

In our standard model, we adopt Eq. (4) to constrain the galaxy SFE (which is kept fixed during the galaxy evolution), given an initial value for the galaxy infall mass, $M_{\rm inf}$ (in the right panel of Fig. 1 the variation of the SFE as a function of the total gas infall mass $M_{\rm inf}$). The role of this assumption will be discussed in Section 5.1.4. We will also consider another case in which a constant SFE as a function of galaxy mass is assumed.

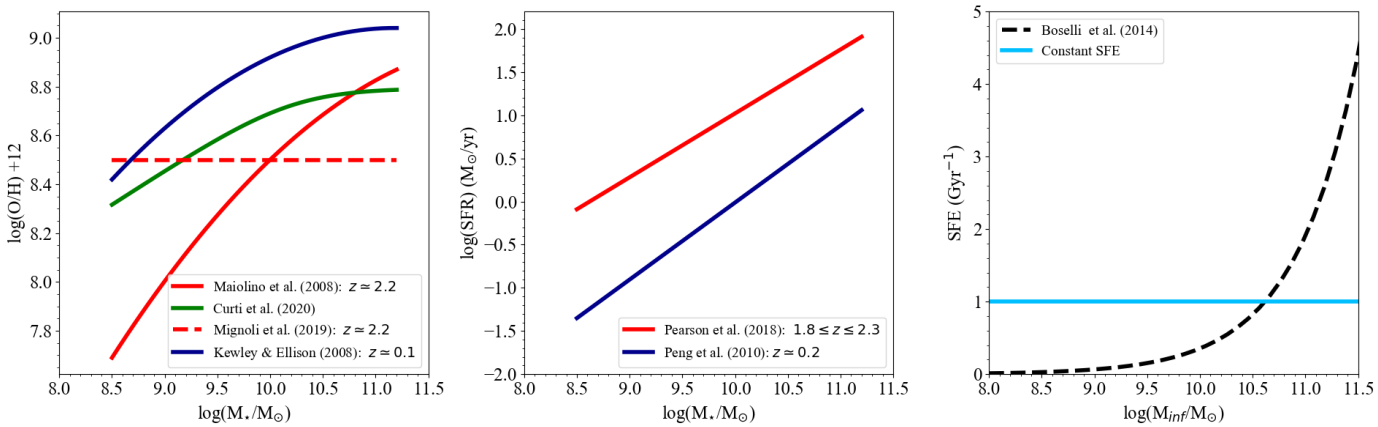

Fig. 1. *Left panel:* Observed MZRs adopted in this paper at different redshifts: the local one by Kewley & Ellison (2008) is depicted with the blue line, the high redshift MZR by Maiolino et al. (2008) with the red one. The red dashed line is the MZR observed by Mignoli et al. (2019) at $z \sim 2$. With the solid green line we also show the local MZR relation for SDSS galaxies found by Curti et al. (2020) with a fully T_e-based abundance scale analysis. *Middle panel:* The star-forming main sequence by Peng et al. (2010) in local SDSS galaxies is shown with the blue line, whereas the high redshift relation is the one by Pearson et al. (2018). *Right panel:* With the dashed black line we show the star formation efficiency as a function of the infall mass M_{inf} from the scaling relation for the gas depletion timescale as found by Boselli et al. (2014). The constant SFE fixed at the value of 1 Gyr^{-1} is indicated with the ligh blue curve.

4. Observed scaling relations at different redshifts

In this Section we describe the observational constraints for the MZR and the star forming MSRs at different redshifts adopted in this work.

The observed MZR at redshift $z \sim 0.1$ is the one by Kewley & Ellison (2008), as fitted by Maiolino et al. (2008) with a calibration based on photoionization models provided by Kewley & Dopita (2002):

$$\log(\mathrm{O/H}) + 12 = -0.0864 \cdot \left[\log\left(\frac{M_\star}{M_\odot}\right) - \alpha\right]^2 + \beta, \quad (5)$$

where α and β are the free parameters of the fit that have been fixed at the values of α=11.18 and β=9.04.

In Section 5.1.5, we will show how our results are sensitive to the adoption of a different calibration method for metallicity measures. In particular, we will show the effects of the adoption of a T_e-based metallicity calibration for the local MZR.

As for the high redshift MZR, we will consider two different relations. The first is the one presented by Maiolino et al. (2008) for galaxies at redshift $z = 2.2$, for which the analytical fit form is the same as Eq. (5) but with $\alpha = 12.38$ and $\beta = 8.99$.

Concerning high redshift objects, Maiolino et al. (2008) underlined that at that time no single strong line calibration method existed over the wide metallicity range spanned by such galaxies. Therefore, at low metallicities ($12 + \log(\mathrm{O/H}) < 8.35$) they adopted calibrations of strong-line diagnostics based on the T_e method, whereas at higher metallicity they relied on photoionization models provided by Kewley & Dopita (2002).

In our analysis, we will also consider the recent results by Mignoli et al. (2019), in which a flat MZR with $\log(\mathrm{O/H})+12 \simeq 8.5$ dex was found for galaxies hosting Type 2 AGN at $z \simeq 2.2$.

Finally, we present the scaling relations of the star-forming main sequence that will be used as a further constraint of our models. At low redshift, the MSR is the one of Peng et al. (2010), computed at redshift $z = 0.2$,

$$\log(\mathrm{SFR/M_\odot yr^{-1}}) = 0.89 \cdot \log\left(\frac{M_\star}{M_\odot}\right) - 8.93. \quad (6)$$

The high redshift ($1.8 \leq z \leq 2.3$) star-forming MSR is the one of Pearson et al. (2018), fitted by the following expression:

$$\log(\mathrm{SFR/M_\odot yr^{-1}}) = 0.74 \cdot \left[\log\left(\frac{M_\star}{M_\odot}\right) - 10.5\right] + 1.39. \quad (7)$$

In the left and middle panels of Fig. 1 we show the observed MZRs and the MSRs used in this work, respectively.

5. Model results

Our aim is to reconstruct the past star formation history of the galaxies which obey the two fundamental scaling relations considered here, i.e. the MZR and the MSR of star-forming galaxies, at two representative different redshifts. The redshifts at which we perform our analysis are those which already include significant samples of star forming galaxies and for which the MZR has been evaluated homogeneously, i. e. using the same method for both the stellar mass and the interstellar metallicity as described in Calura et al. (2009).

The properties of the galaxies who follow the MZR and MSR at such representative redshifts will be studied at different epochs: the backward evolution of the galaxies which obey the observed MZR and MSR at $z \sim 0.1$ and the forward evolution of objects that at redshift $z \sim 2.2$ are part of both the MSR and the MZR. Our aim is to track the evolution of the galaxies which, in a given phase of their history, follow at the same time the MZR and the MSR.

5.1. Backward evolution

5.1.1. The MZR and star-forming MSR at $z = 0.1$

Fig. 2 and Fig. 3 show the backward evolution of the galaxies which obey the analytical fit of the observed MZR at $z \sim 0.1$ of Kewley & Ellison (2008), as reported by Maiolino et al. (2008) and the main sequence of star-forming galaxies as derived by Peng et al. (2010). In Fig. 2 and in Fig. 3, the galaxies are colour-coded as a function of their loading factor λ and infalling gas mass, respectively.

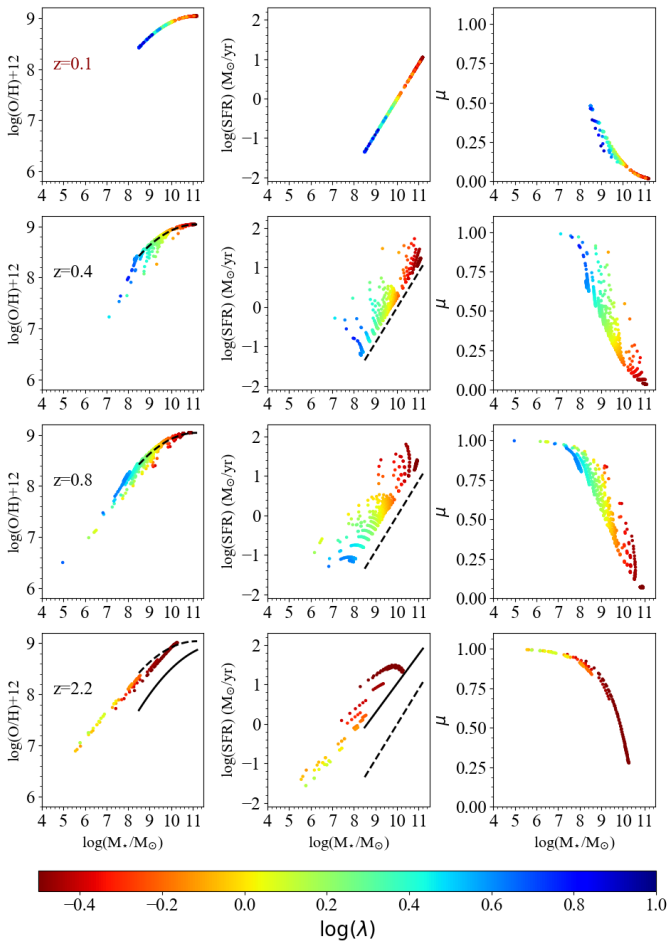

Fig. 2. Backward evolution from $z = 0.1$ to $z = 2.2$ of the galaxies which obey the analytical fit of the observed MZR at $z \sim 0.1$ of Kewley & Ellison (2008), as reported by Maiolino et al. (2008) and the local main sequence of star-forming galaxies as derived by Peng et al. (2010). In the first, second and third column the evolution of MZR, SFR vs stellar mass and gas fraction vs stellar mass evolution are shown, respectively. The colour coding indicates the loading factor parameter λ. The black solid lines in the bottom left- and middle-panels indicate the MZR and MSR observed at redshift $z = 2.2$, respectively. The black dashed lines in the panels of the first column and in each SFR-log($M_\star/M_\odot$) plot, show the MZR at redshift $z \sim 0.1$ of Kewley & Ellison (2008) and the MSR derived in local star-forming galaxies by Peng et al. (2010), respectively.

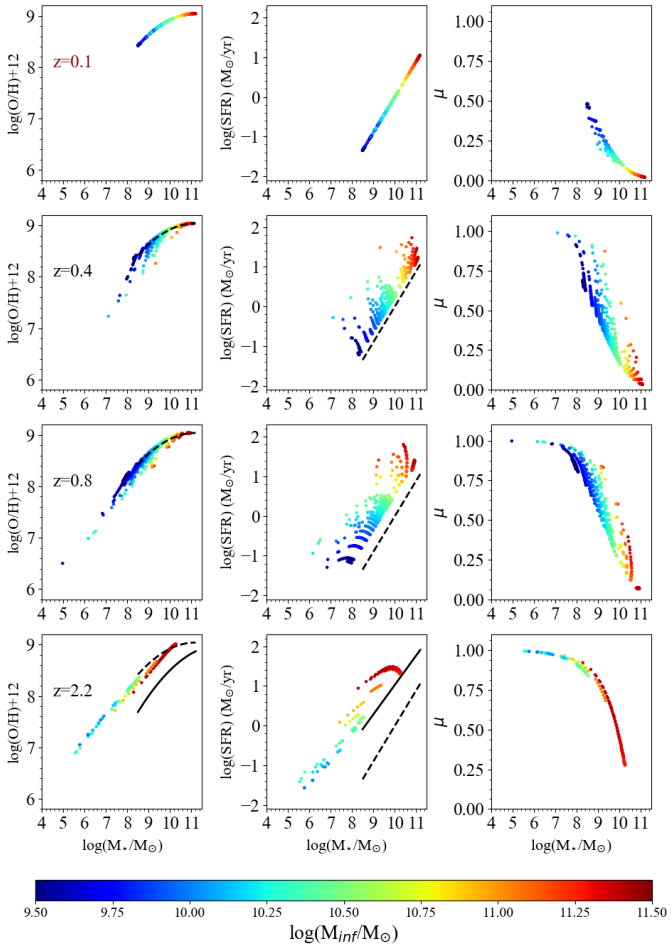

Fig. 3. As in Fig. 2, but the colour coding indicates the total infalling gas mass.

By imposing that they obey the Peng et al. (2010) MSR and by means of the Schmidt (1959) law which links the gas mass to the SFR, we correctly retrieve the anticorrelation between a fundamental quantity related to the gas accretion history of galaxies, i.e. the gas fraction $\mu \equiv M_{gas}/(M_{gas} + M_\star)$, and the stellar mass. It is important to note that such an anticorrelation is a well established, empirical relation of galaxies found at various redshifts. Locally, such anticorrelation was found by Kannappan (2004), who determined the gas fraction for 35,000 galaxies from the Sloan Digital Sky Survey (SDSS) and the Two Micron All Sky Survey (2MASS) databases on the basis of photometric techniques. A similar study on a smaller sample of low-mass galaxies has been performed by Geha et al. (2006), confirming the results of Kannappan (2004). The slope of the curve steepens from low-mass to high-mass systems, which is generally interpreted with decreasing gas consumption timescales from dwarf to giant galaxies (Calura et al. 2008).

The past evolution of our model galaxies has been computed at three different redshifts, i.e. $z = 0.4$, 0.8 and 2.2.
The larger redshift value present in the plot is the one at which a substantial amount of galaxies have appeared, which now are star-forming and build the local MZR. The epoch at which each galaxy must be born is a result of our method, and which stems directly from Eq. 1 and from the imposition of the observational constraints.
A significant evolution of all the three quantities shown in Fig. 2 is evident from the plot. A positive correlation between stellar mass and metallicity is already in place at $z = 2.2$. In the young galaxies present at that redshift, the shape of the MZR is missing the characteristic plateau at large masses which is generally observed at all redshifts.

This can be understood considering that the one at $z = 2.2$ as shown in Fig. 2 is only a sub-sample of the entire population of all the star-forming galaxies at that redshift, which will obey the MZR but which will include also many systems which now are passive, i.e. which do not belong to the local MSR relation, and which build the high-mass plateau at that redshift, as shown in Savaglio et al. (2005) and Maiolino et al. (2008).

The relation between SFR and mass appears appreciably flatter than at $z = 0.1$, and even if the gas fraction still anti-correlates with the stellar mass, it is characterised by an inverted curvature with respect to the local relation. All the galaxies building the three relations are characterised by very low wind ef-

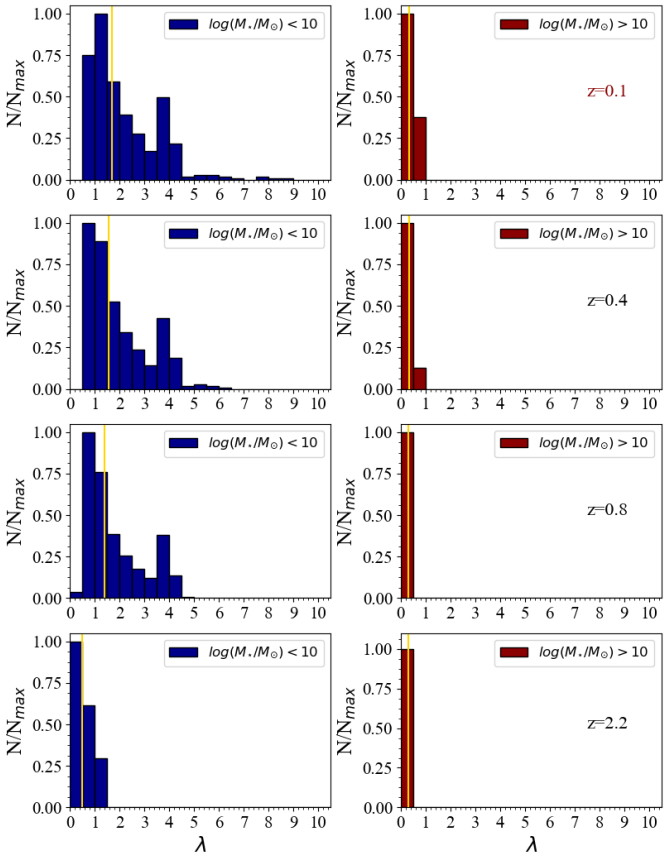

Fig. 4. Distribution of the loading factor parameter λ for the galaxies of Fig. 2 computed at redshifts $z = 2.2$, $z = 0.8$, $z = 0.4$, and $z = 0.1$ for 2 different bins of stellar mass. The left panels show distributions for objects with stellar mass $log(M_\star/M_\odot) < 10$, and right panels indicate distributions for stellar mass $log(M_\star/M_\odot) > 10$. The yellow vertical lines indicate the median values of each distribution.

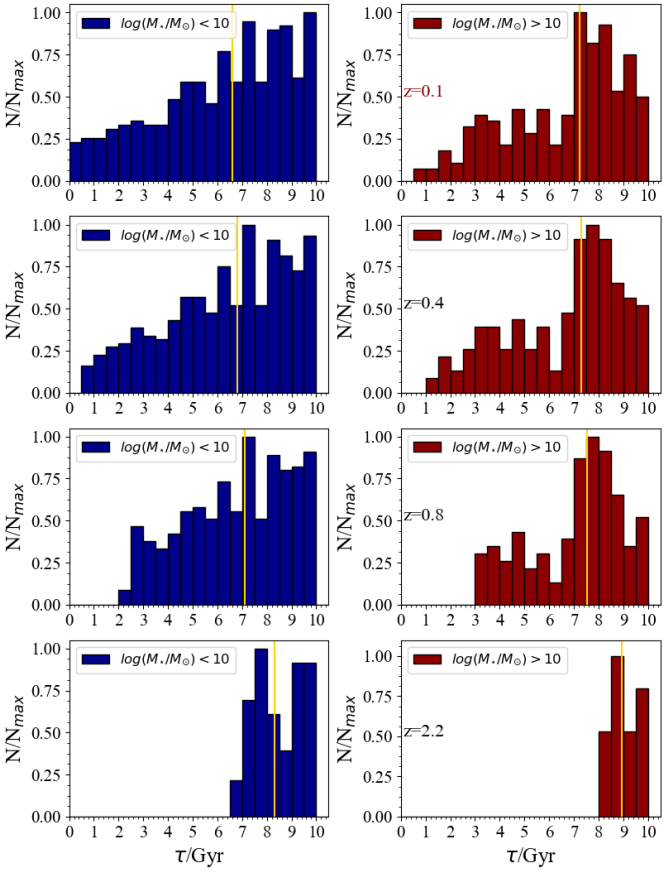

Fig. 5. As in Fig. 4, but in each panel the plotted distribution is for the infall time-scale parameter τ.

ficiencies ($\log(\lambda) \leq -0.4$) and by the large infall mass values ($\log(M_{inf}/M_\odot) \sim 11.5$).

At $z = 0.8$, the MZR appears more extended than at $z = 2.2$, in particular in that it is much more populated at $\log(M_\star/M_\odot) \geq 8$. At this redshift, the hint of a plateau has already appeared in the MZR at the highest mass values, namely at $\log(M_\star/M_\odot) > 10$. The appearance of the plateau may be interpreted with a flattening of the star formation history of the most massive galaxies, which are characterised by the largest SFR values and shortest gas consumption timescales (see Fig. A.6). As a consequence of a faster gas consumption in the largest galaxies, their present-day metallicity is reached at earlier times than in low-mass galaxies.

Also the SFR-M_* relation of the galaxies at $z = 0.8$ is more extended and more scattered than at $z = 2.2$.

The $\mu - M_\star$ relation sees the appearance of a significant population of newly born, extremely gas-rich and metal-poor galaxies characterised by $\mu \sim 1$ at $\log(M_*/M_\odot) < 8$. Also the range of the wind parameter and infall mass values presented by the galaxies at $z = 0.8$ have extended considerably with respect to $z = 2.2$. The maximally gas-rich galaxies present the largest values of the λ parameter ($\log \lambda \sim 0.6$) and are also characterised by the lowest infall mass values.

On the other hand, the strong evolution experienced by the largest systems leads them to keep their gas fractions very low.

At $z = 0.4$ the horizontal extension of the the MZR has reduced, as all galaxies have grown in stellar mass. The MZR is now much more similar to the local one, with the exception of a larger scatter at low masses which, by construction, later on will disappear. The population of galaxies with gas fractions ~ 1 have considerably reduced. The gas fraction-mass relation shows a parabolic behaviour at the largest stellar masses, with an inflection at $\log(M_*/M_\odot) \sim 9$.

In Figs. 4 and 5, we present the distribution of the loading factor parameter λ and the infall time-scale parameter τ at different redshifts for the model galaxies of Figs. 2 and 3. The distribution are computed in two different bins of stellar masses ($M_\star < 10^{10} M_\odot$ and $M_\star > 10^{10} M_\odot$).

The galaxies present at redshift $z = 2.2$ are characterized by weak winds and long time scales of gas accretion. In fact, at low redshift these objects have to maintain a large reservoir of gas in order to be part of the local MSR.

Galaxies in the larger mass bin show very weak winds and very little evolution of both the median λ and τ values.

We note that galaxies characterized by $M_\star < 10^{10} M_\odot$ at redshifts $z < 2.2$ maintain their stellar mass below this value during their entire evolution up to redshift $z = 0.1$, as visible in Fig. 2 and 3.

From Fig. 5 we see that the low edge and the median of the infall time-scale distribution decrease with decreasing redshift in both stellar mass bins. This reflects that at each redshift, the galaxies - among the ones that are on the local MZR and MS - with short time-scales of accretion τ and/or high loading factors did not exist yet at high z.

In the lowest mass bin, a decrease of the median τ is accompanied by an increase of the median λ value. This reflects the fact

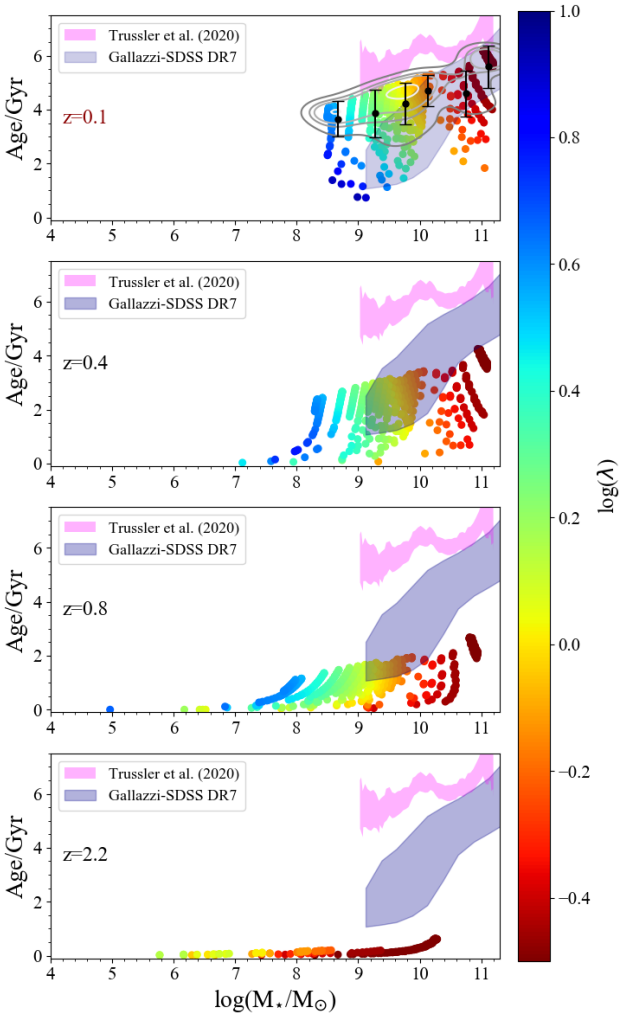

Fig. 6. Backward evolution of the mass-weighted age versus stellar mass relation (computed at $z = 2.2$, $z = 0.8$, and $z = 0.4$) for the galaxies which lie on the MZR of Kewley & Ellison (2008) and on the MSR as derived by Peng et al. (2010). The colour coding indicates the loading factor parameter λ. The white-grey contour lines indicate isodensity contours. The shaded pink area indicates the observational data by Trussler et al. (2020) for local star-forming galaxies ($0.02 < z < 0.085$), whereas the shaded blue area stands for the relation obtained using the SDSS-DR7 catalog of mass-weighted ages estimated as in Gallazzi et al. (2008) using the same selection of star-forming galaxies as Trussler et al. (2020). In the upper panel, the black points are the mean age values of the simulated galaxies at redshift $z \sim 0.1$ inside bins of size 0.5 $\log(M_\star/M_\odot)$ and the error bars are the standard deviations.

that a larger amount of mass with respect to more massive systems needs to be expelled to keep their metallicity at low values and to still have them on the MZR.

The median values of the infall time scale τ at redshift $z = 0.1$ are 6.59 Gyr for galaxies with $M_\star < 10^{10} M_\odot$ and 7.25 Gyr for $M_\star > 10^{10} M_\odot$, respectively (see Fig. 5). Such values are larger than the ones found in star forming galaxies by Spitoni et al. (2017b), in which 75 % of the galaxies showed infall time scales smaller than 6 Gyr. The difference is due to the fact that here we impose that the galaxies have to follow simultaneously the MZR and the MSR, whereas in Spitoni et al. (2017b) the only requirement beside the MZR was a specific SFR value above a given threshold, which was $2.29 \times 10^{-11} \mathrm{yr}^{-1}$.

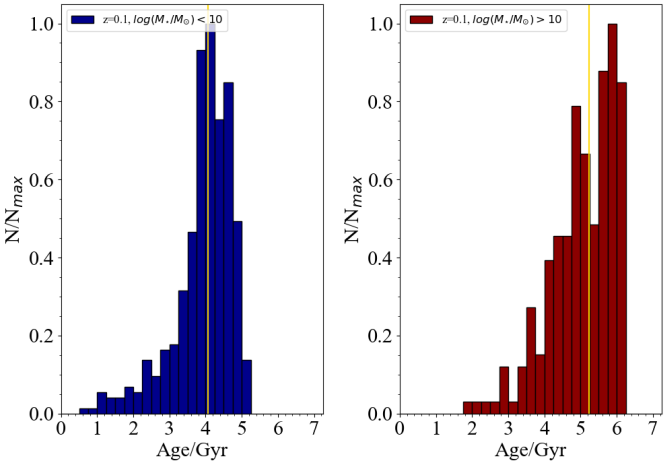

Fig. 7. Age distribution computed at redshift $z = 0.1$ for the galaxies which lie on the MZR of Kewley & Ellison (2008) and on the MSR as derived by Peng et al. (2010) in two different mass bins, $log(M_\star/M_\odot) < 10$ (left) and $log(M_\star/M_\odot) \geq 10$ (right). In each panel, the yellow vertical line indicates the median value of the distribution.

More massive galaxies on the MSR have larger SFRs, and as already mentioned, only these systems can afford the longest time-scales of accretion, which allow them to exhibit large SFR values down to $z = 0.1$.

5.1.2. Downsizing and scaling relations

Fig. 6 shows the backward evolution of the age versus stellar mass relation for galaxies which at $z \sim 0.1$ obey the MZR and the main sequence of star-forming galaxies.

Approximately, 89.2 % of the simulated galaxies are located in the region enclosed by the most external contour line in the upper panel of Fig. 6. Such a positive relation between age and stellar mass is retained also if we increase the resolution of our parameter grid (λ, τ) by a factor of two. We notice that the positive correlation between age and stellar mass is preserved at any redshift.

From the age distributions computed at redshift $z = 0.1$ for the two range of stellar masses (see Fig. 7) we infer that the predicted median age of star-forming systems are ~ 4.06 Gyr (lower stellar mass bin) and 5.23 Gyr (high stellar mass bin).

The simulated galaxies at redshift $z = 0.1$ reproduce the slope of the observed age-mass relation for star-forming galaxies as found by Trussler et al. (2020). However, the predicted ages are systematically ~ 1 Gyr younger than the Trussler et al. (2020) ones.

We also compare the predicted age-mass relation with the one obtained adopting the mass-weighted ages estimated as in Gallazzi et al. (2008) for SDSS-DR7 (Gallazzi et al. 2020, in prep - see also Pasquali et al. 2019). From the Gallazzi-DR7 catalog we select star-forming galaxies with the same criterion as Trussler et al. (2020) and over their same redshift interval. The Gallazzi relation is steeper and overall shifted to lower mass-weighted ages than the estimates by Trussler et al. (2020).

The noticeable differences in both normalization and slope of the Gallazzi age-mass relation and the Trussler et al. (2020) relation can originate from different assumptions in the observational estimates of ages: i) the Bruzual & Charlot (2003) SSP models in comparison to Maraston & Strömbäck (2011), ii) the use of a stochastic library of parametric SFHs compared to a lin-

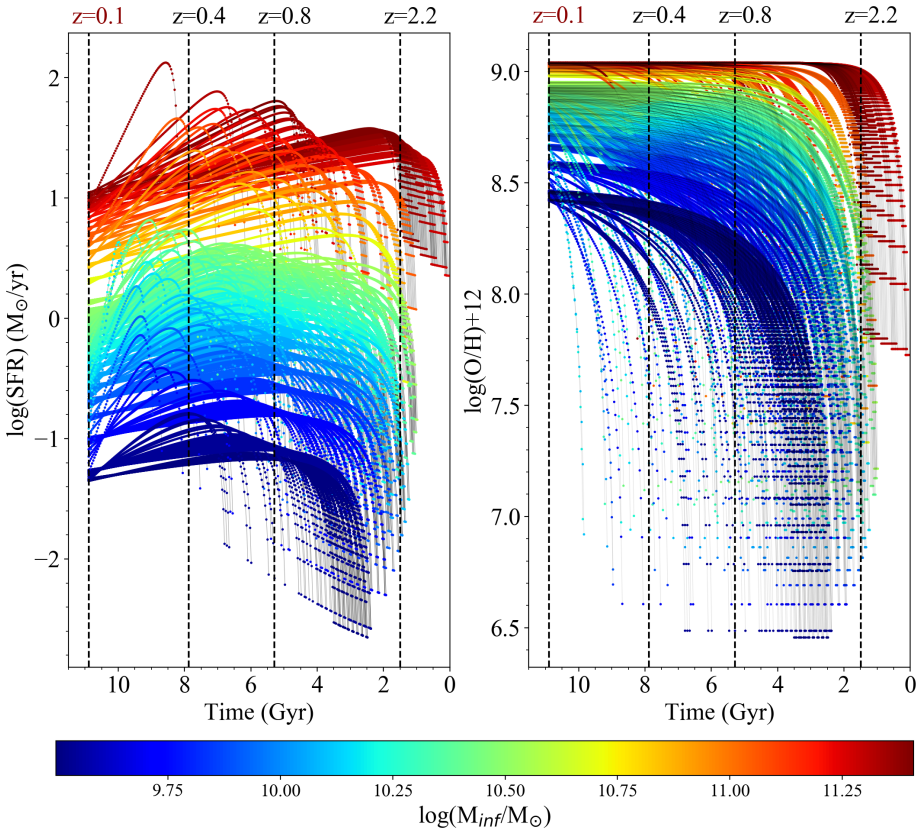

Fig. 8. Evolution of star formation rate (left panel) and oxygen abundance (right panel) as a function of time for the galaxies which lie on the MZR of Kewley & Ellison (2008) and on the MSR as derived by Peng et al. (2010). The colour coding represents the infall mass.

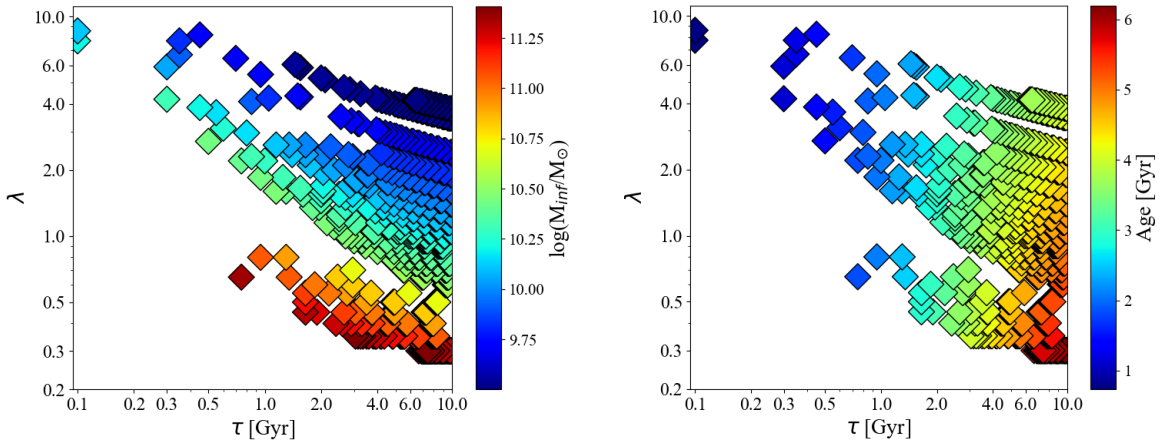

Fig. 9. Parameter space analysis (wind parameter λ versus infall time scale τ) of the galaxies which line on the MZR of Kewley & Ellison (2008) and on the main sequence of star-forming galaxies as derived by Peng et al. (2010). In the left panel the colour coding represents the infall mass, whereas in the right one it represents the galactic age.

ear combination of SSP without assuming a functional form for the SFH, translating into differences in the allowed fraction of old stars, iii) limiting the formation age of the models to the age of the Universe compared to allowing SSPs as old as 15 Gyr, iv) a Bayesian statistical approach compared to a χ^2-minimization code. While it is clear that a quantitative description of the mass-weighted age relation with mass is subject to the observational method adopted, both determinations agree in indicating a positive correlation.

Fig. 6 implies a key result, i. e. that galactic downsizing as reflected from the ages of their stellar populations is naturally accounted for by systems that obey two fundamental scaling relations, namely the MZR and the MSR. It is worth noticing that assuming two scaling relations with zero scatter, those together predict an age-mass relation with intrinsic scatter ($\sim$ 0.8 Gyr). This means that there might be a variety of SFHs that can lead to the current equilibrium between SFR and metal enrichment.

The DS of galaxies is also visible from the temporal evolution of the SFR and oxygen abundances of the model galaxies as shown in Fig. 8. In this figure, the evolution of each quantity is shown for systems of different masses as a function of time, for an evolutionary interval of $\sim$ 10.5 Gyr.

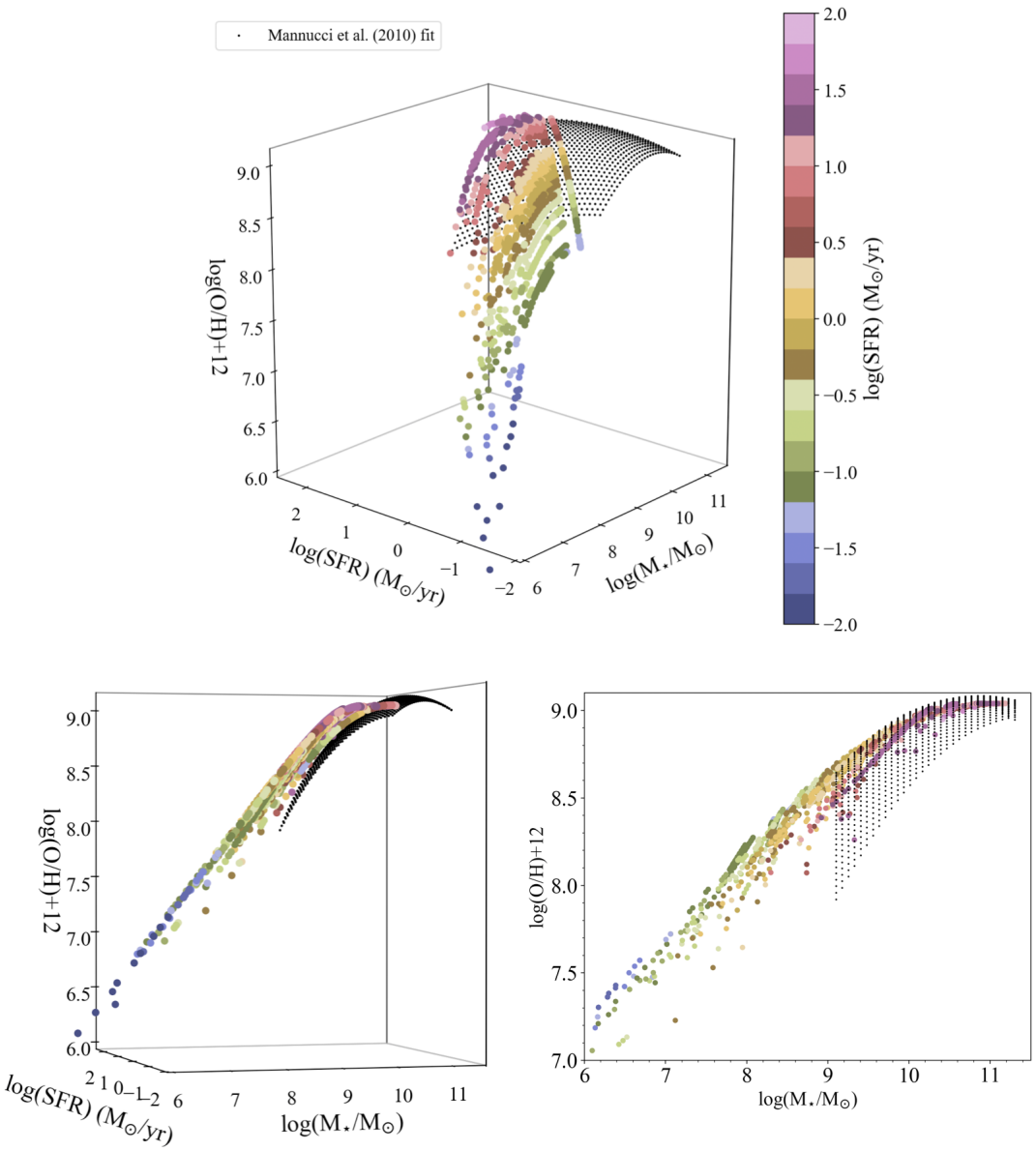

Fig. 10. Three projections of the Fundamental Metallicity Relation of Mannucci et al. (2010) compared with the properties of the ancestors of the galaxies that at z=0.1 follow the MSR and MZRs. The big solid circles are the model galaxies illustrated in Section 5.1.1, and for which the SFR, stellar mass and metallicity values reported in the plots are computed at z=0.1, 0.4, 0.8, 1.5 and 2.2, colour-coded as a function of their SFR values. The small black dots are a second-order fit of the SDSS data as presented in Mannucci et al. (2010).

These plots show that the bulk of the stars of the galaxies belonging to the highest mass end ($\log(M_{inf}/M_\odot) > 11$) of the MZR must have formed at early times. In most of these systems the SFH peaks soon after their formation and their metallicity saturates at its maximum value ($12 + \log(O/H) \sim 9$) after ~ 1 Gyr of evolution. Some high-mass galaxies may be characterised by SFHs which peak at more recent epochs (i.e. at ages < 4 Gyr), and present SFR values larger than the ones of the older galaxies. The systems also have short infall timescales and populate the lowest τ- (< 6 Gyr) tail of the infall timescale distribution. Moreover, they present λ values larger than their older analogues but still < 1 (see later), implying that galactic outflows are not the main driving mechanisms of their evolution.

From Fig. 8, we see that the lower the stellar mass of the galaxies, the lower the age at which the SFH peaks and the slower the growth of the metallicity with time. Our analysis of the star formation history of these galaxies is in agreement with the one presented in other works (Maiolino et al. 2008; Calura et al. 2009) based on studies of the MZR, although the MZR alone does not necessarily imply galactic downsizing. In order to account for it one must impose simultaneously the MZR and the MSR. This represents one major result of the present work. With our models, it is also easy to show how the positive correlation between age and mass presented in Fig. 6 disappears completely if we impose that galaxies must follow the MZR only.

As mentioned in Section 3, in our model the temporal evolution of the SFH can be well approximated with a function proportional to $te^{-t/\tau}$ (see discussion in Weinberg 2017). Hence, adopting this analytical expression, the mass weighted age presented in Eq. (3) computed at the time t_n can be rewritten as follow:

$$\mathrm{Age}_{\mathrm{approx}}(t_n) = \frac{t_n}{1 - e^{-t_n/\tau}} - \tau. \quad (8)$$

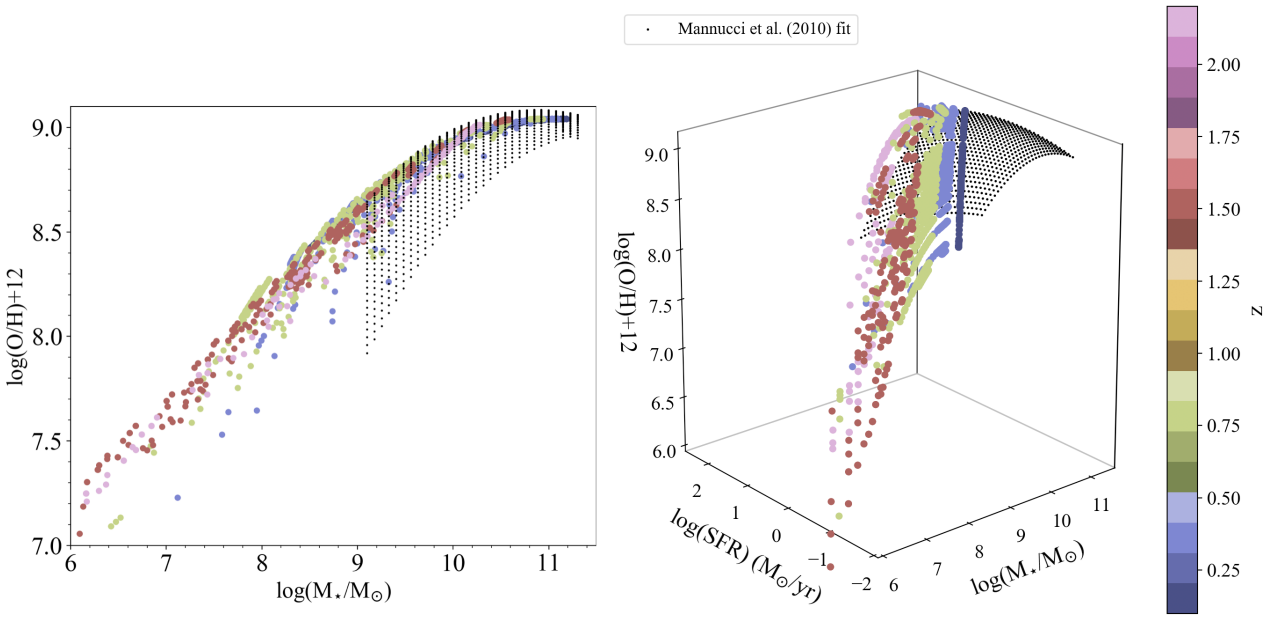

Fig. 11. Two projections of the Fundamental Metallicity Relation of Mannucci et al. (2010) compared with the properties of the model galaxies as in Fig. 10, colour-coded as a function of their redshift z.

In Fig. 8, we note that the oldest galaxies have been evolving for roughly $t_n \simeq 10.5$ Gyr. Moreover, these objects are characterized by long time-scale of accretion τ, and a representative value is $\tau \simeq 9.5$ Gyr (see Fig. 5). Substituting these quantities in the approximated mass-weighted age introduced above in Eq. (8), we find a value of $\mathrm{Age}_{\mathrm{approx}}(t_n) = 6.19$ Gyr, in perfect agreement with our results for the oldest objects as reported in Fig. 6.

To better understand the main reason for the results discussed here, in Fig. 9 we show the loci occupied by our galaxies in the space of the free parameters of our model, i. e. λ and τ. The most massive objects are the oldest ones, which are generally located in the bottom-right corner of the plots and which are characterized by longest accretion timescales and smallest values for the wind parameter. A population of young, very massive systems is visible in Fig. 9, which are the galaxies with the largest SFR values of Fig. 8. In Fig. 9, such systems are considerably underdense with respect to their older analogues. This occurs because, in order to follow both the MZR and MSR, only a very limited range of values in the λ-τ space will be allowed. In this particular region of this space, small perturbations of the values of each of these parameters will be enough to drive galaxies off one (or both) of the two fundamental scaling relations, which explains the paucity of points with $\tau \sim 1$ Gyr and $\lambda \sim 0.8$. On the other hand, a larger range and larger variations for each parameter will be admitted in the bottom-right corner, where massive system tend to cluster.

In galaxy evolution models, some properties which reflect galactic DS can generally be accounted for in different ways and acting on various parameters, i. e. by varying the stellar IMF (Calura & Menci 2009), or by varying the SF efficiency in galaxies of various mass (Matteucci 1994). In the next section we will discuss further the role of this parameter in particular, as well as the implications on our results.

5.1.3. The Fundamental metallicity relation of Mannucci et al. (2010)

Mannucci et al. (2010) showed that star forming galaxies lie on a tight surface in a 3D space defined by stellar mass, gas-phase metallicity, and SFR. The median values of metallicity of the SDSS galaxies can be expressed by means of a second-order polynomial fit in $\mathrm{M}_\star$ and SFR:

$$12 + \log(\mathrm{O/H}) = 8.90 + 0.37m - 0.14s - 0.19m^2 + 0.12ms - 0.054s^2 \quad (9)$$

where m=log($\mathrm{M}_\star/\mathrm{M}_\odot$)-10 and s=log(SFR).

In our study we analyze only a subsample of those local SDSS galaxies that, by construction, lie at redshift $z \sim 0.1$ on a curve in this 3D space, represented by the combination of the MSR and MZR.

However, we can test whether the ancestors of these galaxies lie or not on the hyper-surface defined by the FMR. In fact, the Mannucci et al. (2010) relation has been defined "fundamental" implying that, in principle, it has to be valid at all redshifts.

In Figs. 10 and 11 we compare in the 3D space defined by M_*, SFR and metallicity the properties of the model galaxies computed at redshift $z = 0.1, 0.4, 0.8, 1.5, 2.2$ with the FMR of Mannucci et al. (2010), color coded as a function of SFR and redshift, respectively.

Figs. 10 and 11 show that in this 3D space, our galaxies lie on a surface which is in reasonable agreement with the FMR determined by Mannucci et al. (2010).

5.1.4. Downsizing and the star formation efficiency

In this Section we discuss the robustness of our results in accounting for galactic downsizing with respect to the SF efficiency, one key parameter of chemical evolution models. As discussed in Section 1, an increase of the SFE as a function of mass is often invoked in chemical evolution models to explain galactic

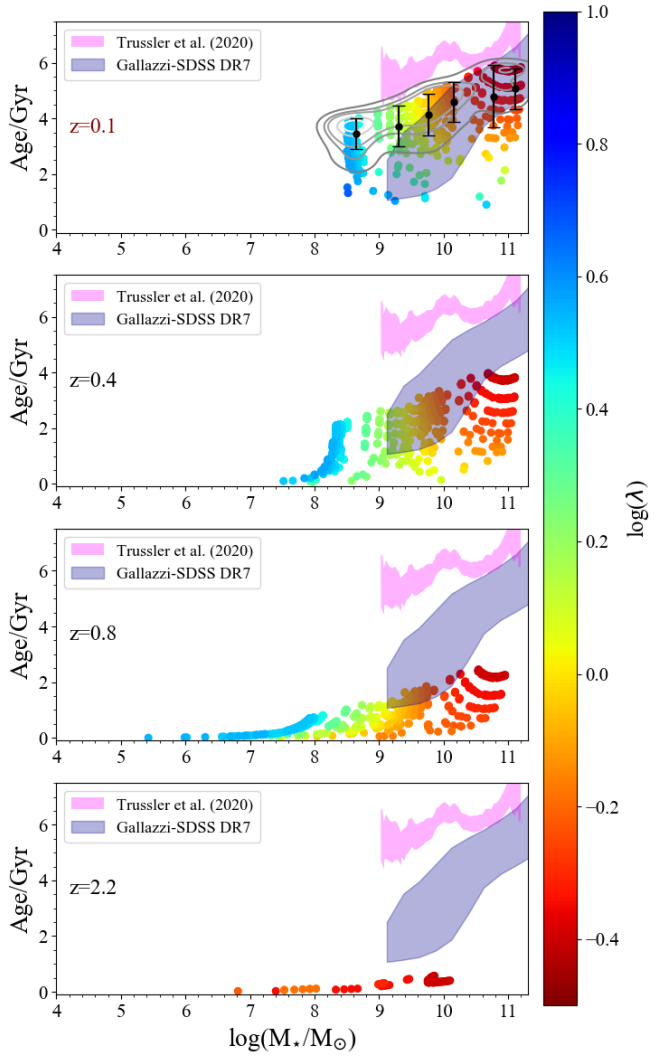

Fig. 12. As in Fig. 6 but computed assuming a constant SFE fixed at the value of 1 Gyr^{-1}.

DS, in particular as traced by the integrated stellar [α/Fe] abundance of the stellar populations of local elliptical galaxies (Matteucci 1994; Pipino & Matteucci 2011).

As introduced in Section 3, we assume the relation of Boselli et al. (2014) between SFE and galaxy mass, where in our case the stellar mass is replaced by the infall mass M_{inf} (as done also in Spitoni et al. 2017b). However, this assumption is not key for our results, in particular as far as the capability of our models to account for the age vs stellar mass relation is concerned. To show this, we present the results obtained by adopting a constant SFE=1 Gyr^{-1}, i.e. independent on the mass of the galaxy. In the right panel of Fig. 1, we show the SFE as a function of the infalling gas mass used here and adapted from the Boselli et al. (2014) scaling relation compared to a constant value of SFE=1 Gyr^{-1}. As visible from Fig. 1, the variable SFE spans a large range, between 0.01 and 4.5 Gyr^{-1}. The relation of Boselli et al. (2014) presents SFE$\sim$ 1 Gyr^{-1} at mass values $\sim 10^{10.5}$ $M_{\odot}$, with a factor $\sim$ 4.5 variation between the value at this mass up to the one of galaxies ten times more massive. We also note that low mass systems can have SFE values which are lower even by a few orders of magnitude.

In Fig. 12 we present the galactic age-stellar mass relation at different redshifts computed for the galaxies that at redshift z =

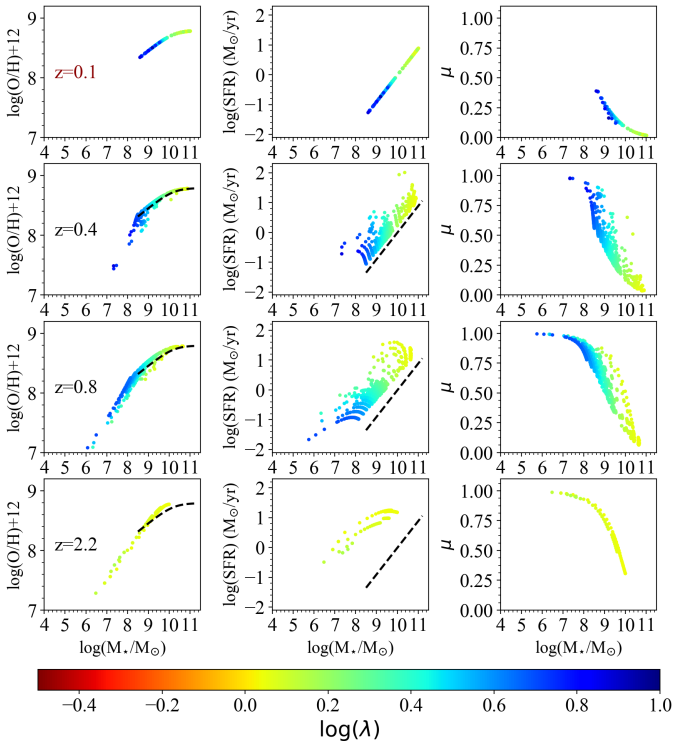

Fig. 13. Backward evolution from z = 0.1 to z = 2.2 of the galaxies which obey the analytical fit of the observed MZR at $z \sim 0.1$ of Curti et al. (2020) and the local main sequence of star-forming galaxies as derived by Peng et al. (2010), colour coded as a function of the loading factor parameter λ as in Fig. 2. The black dashed lines in the panels of the first column and in each SFR-log(M$_{\star}$/M$_{\odot}$) plot, show the MZR of Curti et al. (2020) and the MSR derived in local star-forming galaxies by Peng et al. (2010), respectively.

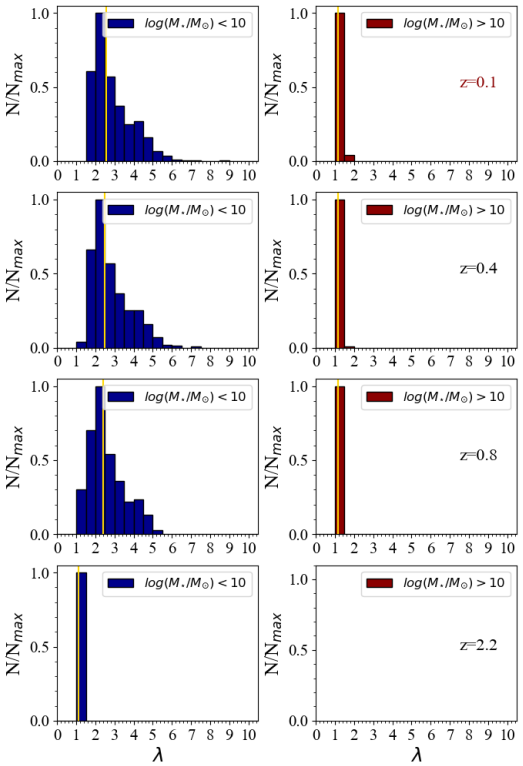

Fig. 14. As in Fig. 4, but computed with the local MZR proposed by Curti et al. (2020).

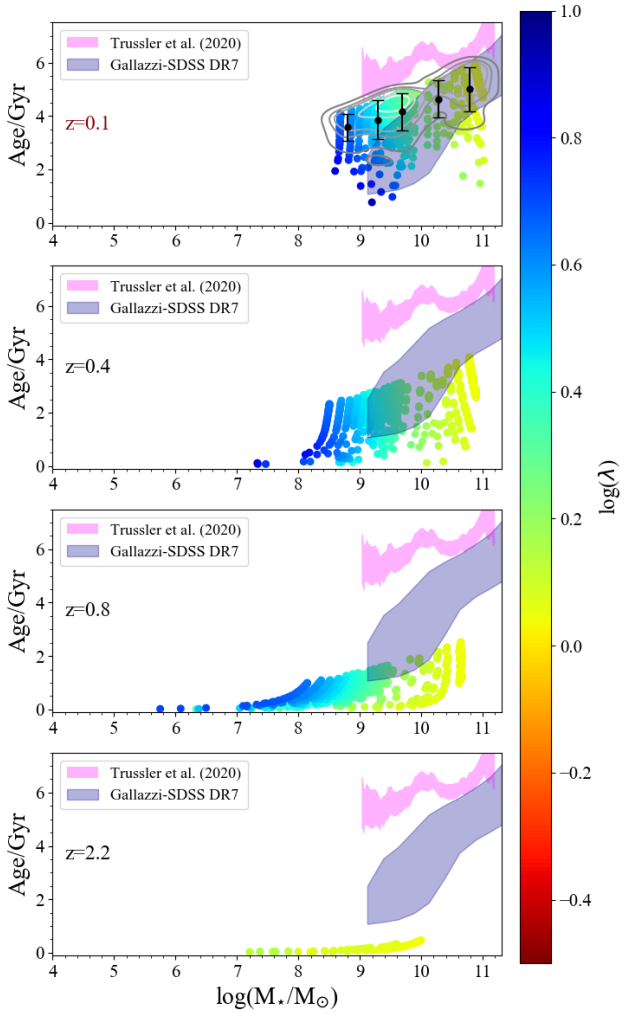

Fig. 15. As in Fig. 6, but computed assuming at redshift $z \sim 0.1$ the MZR proposed by Curti et al. (2020).

0.1 are part of the star-forming main sequence and of the MZR, but assuming a constant SFE of 1 Gyr^{-1}, a value which is typical for chemical evolution models of Milky Way-like galaxies.

A clear DS in the galaxy models is still evident even assuming a constant SFE, in that on average, the larger the stellar mass, the older their stellar populations. This confirms that our main result, namely that galaxies that lie on both the MZR and MSR will also necessarily be characterised by a downsizing in their stellar populations, is independent from the adopted star formation efficiency. To our knowledge, this is the first time that this result is derived theoretically.

5.1.5. The effect of a fully T_e-based abundance scale for galaxies

Curti et al. (2017) presented new empirical calibrations for strong-line diagnostics of gas phase metallicity in local star forming galaxies by uniformly applying the T_e method over the full metallicity range probed by the SDSS. Moreover, a MZR for local SDSS galaxies obtained with the T_e-based method was presented.

The new fit of the median MZR for the SDSS sample is the following:

$$12 + \log(O/H) = Z_0 - \gamma/\beta * \log\left(1 + \left(\frac{M_\star}{M_0}\right)^{-\beta}\right), \quad (10)$$

where $Z_0 = 8.793$, $\log(M_0/M_\odot) = 10.02$, $\gamma = 0.28$ and $\beta = 1.2$. From the left panel of Fig. 1, it is clear that the slope and overall normalisation of the MZR are sensitive to the calibration method (see also Kewley & Ellison 2008), and that the relation obtain by Curti et al. (2017) is flatter and generally characterised by lower metallicity values than the one of Kewley & Ellison 2008.

In this Section, we test whether the assumption of a purely T_e-based MZR also affects the main results presented above.

Figures 13, 14 and 15 show results qualitatively similar to the ones of Figs, 2, 4 and 6, respectively. The MZR of Curti et al. (2020) produces stronger winds than Kewley & Ellison (2008) MZR (Figs. 13 and 14). This result can be ascribed to the smaller oxygen abundances of the galaxies which follow the Curti et al. (2020) MZR, as in the framework of the present work, it is by means of stronger winds that galaxies can have a lower metal content than the models computed when the Kewley & Ellison (2008) MZR was assumed.

Fig. 15 shows that also galactic downsizing is preserved when the Curti et al. (2020) MZR is used, with a predicted age-mass relation very similar to the one of Fig. 6.

5.2. Forward evolution

5.2.1. The MZR by Maiolino et al. (2008) and MSR at $z = 2.2$

In this work we are also interested in the evolution of galaxies that at high redshift are part of both the main sequence and of the MZR. As for the MZR, the observational constraint we discuss here is the one by Maiolino et al. (2008), whereas the star-forming MSR is the one by Pearson et al. (2018) for galaxies observed in the redshift range $1.8 \leq z \leq 2.3$.

In the middle panel of Fig. 1 we compare the local MSR with the one at high redshift by Pearson et al. (2018). Large differences characterize the two sequences, in particular as far as the zero-point of the relation is concerned. An offset by at least one order or magnitude in SFR is visible for instance at stellar masses $\log(M_\star/M_\odot) \sim 11$, whereas any variation in the slope is much less appreciable. Such a difference in normalization is expected from the evolution of the cosmic star formation rate density (e. g., Madau & Dickinson 2014) and comparable to what found in other studies (e. g., Santini et al. 2017). The MZR considered in this section (solid thick red line in the left panel of Fig. 1) is steeper than the local one (solid thick blue line) and, as discuss by Maiolino et al. (2008), this might imply different evolutionary time-scales in galaxies of different masses.

In Fig. 16 we show the 'forward' (i. e. evolved towards lower redshifts, corresponding to later epochs) evolution of the galaxies which at $z = 2.2$ obey the MZR and MSR, computed at $z = 2.2$, $z = 0.8$, $z = 0.4$, $z = 0.1$.

The large SFR values required by the high redshift MSR and the associated small oxygen abundances of the MZR relation force the galactic systems to be subject to stronger winds and assembled on shorter time-scales compared to the galaxies presented in Section 5.1.1 (see Fig. 17). Hence, galaxies suffer strong depletion of gas and evolve passively at the redshifts $z < 2.2$. In Fig. 16, it is evident that the gas fraction drops dramatically from redshift $z = 2.2$ to redshift $z = 0.8$. The most massive objects show high stellar masses (built up in a short time) and high metallicity and must have consumed

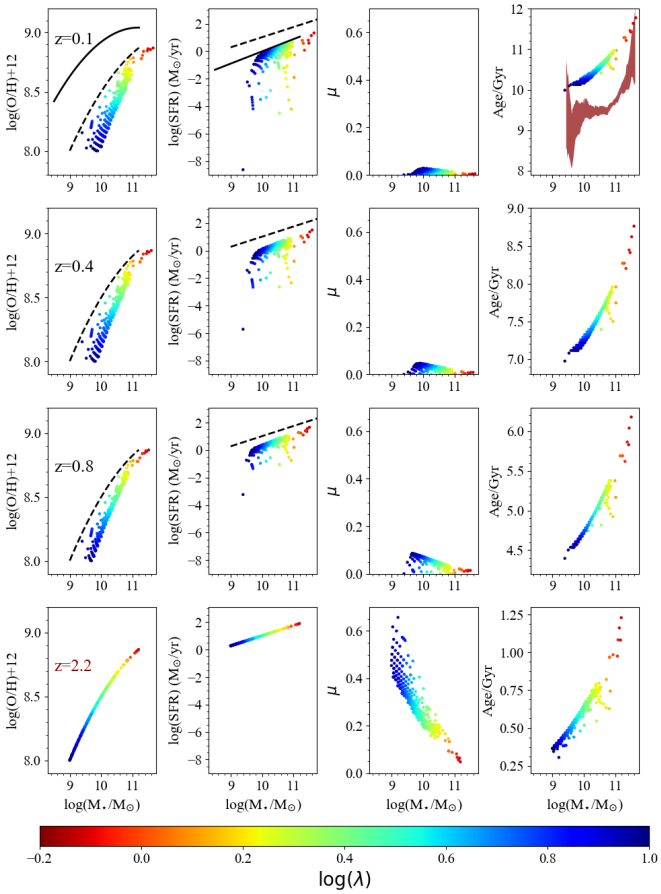

Fig. 16. Forward evolution from $z = 2.2$ to $z = 0.1$ of the galaxies which obey the analytical fit of the observed MZR at $z \sim 2.2$ by Maiolino et al. (2008) and the main sequence of star-forming galaxies as derived by Pearson et al. (2018). Starting from the left, in the first, second and third column the evolution of the MZR, SFR vs. stellar mass and gas fraction vs stellar mass are shown, respectively. In the last column, the age-stellar mass relation is shown. The colour coding indicates the loading factor parameter λ. The black dashed lines in the panels of the first column and in each SFR-log($M_\star/M_\odot$) plot, show the MZR at redshift $z \sim 2.2$ of Maiolino et al. (2008) and the MSR derived in high redshift star forming galaxies by Pearson et al. (2018), respectively. The thick, black solid lines in the first two top-left panels are the MZR at redshift $z \sim 0.1$ of Kewley & Ellison (2008) and the MSR of Peng et al. (2010), respectively. In the upper-right panel with the dark red shaded area we also include the age-stellar mass relation for the local passive galaxies by Trussler et al. (2020).

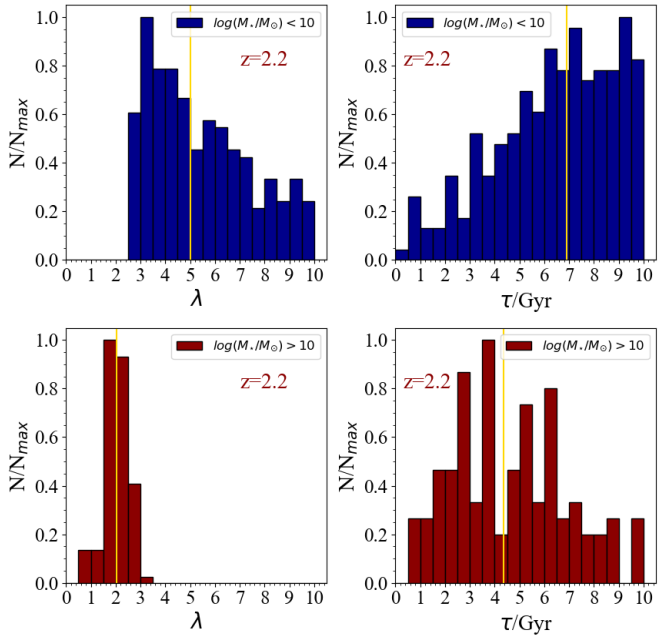

Fig. 17. Distribution of the predicted galaxies of Fig. 16 in terms of the loading factor parameter λ (left panels) and the infall time-scale parameter τ (right panels), computed at redshift $z = 2.2$ for different stellar mass bins.

their reservoir of gas soon after redshift $z = 2.2$. After that, the buildup of their stellar mass and metals was already complete, and they have undergone little evolution at later times. Less massive galaxies, characterized by stronger winds (see Fig. 17), present a more sensible evolution, which manifests in a steepening of the MZR towards recent times. In conclusion, the forward evolution of the single galaxies in the MZR relation is characterized by an "horizontal" evolution at roughly constant metallicity.

The passive evolution of these galaxies can be also inferred by the their age-stellar mass relation at redshift $z = 0.1$, which is similar to the one followed by local passive galaxies of Trussler et al. (2020). However, passive galaxies in Trussler et al. (2020) have much larger stellar metallicities than simulated galaxies at redshift $z = 0.1$. In principle, these galaxies could have been part of the local passive sequence of Trussler et al. (2020) as due to a quenching mechanism, such as the one proposed by Peng et al. (2015): e.g. by "strangulation" (see their lower panel in Fig.1). After the beginning of the "strangulation" no outflow and no gas accretion affect the galactic system and the star formation can continue with the gas available in the galaxy until it is completely used up. During this phase the gas metallicity increases substantially because of the lack of dilution from inflowing gas and gas loss.

As already underlined by Maiolino et al. (2008), galaxies belonging to the MZR observed at different redshifts should not be seen as an evolutionary sequences. In fact, Fig. 17 clearly shows that at redshift $z = 2.2$ these galaxies are characterized by stronger winds compared to the galaxies studied in Section 5.1.1. This is a result of imposing that they also belong to the MSR which, at $z = 2.2$, on the entire stellar mass range is characterised by larger SFR values than the one low redshift. In order to present at the same time low metallicities and high SFR values, it is clear that galaxies at $z = 2.2$ must have suffered much stronger stellar winds than galaxies belonging to the MZR and MSR at lower redshifts.

In Fig. 18 we compare the properties of the galaxies which at redshift $z \sim 2.2$ follow the MZR and MSR relations with the FMR of Mannucci et al. (2010). The models shown in Fig. 18 are computed at redshifts $z = 0.1, 0.4, 0.8, 2.2$, and color-coded as a function of z. The loci occupied by the model galaxies partially overlap with the FMR only at $z = 2.2$, whereas at lower redshifts the fall off the surface traced by the black points, which represent the analytical fit to the FMR presented in Sect. 5.1.3. This due to the fact that galaxies which at $z = 2.2$ follow both MZR and MSR become passive at later times, as shown by the progressive decline of their SFR values.

5.2.2. The MZR by Mignoli et al. (2019) and MSR at $z = 2.2$

In the narrow line regions (NLR) of a sample of 88 C IV-selected objects containing type 2 AGNs, Mignoli et al. (2019) measured

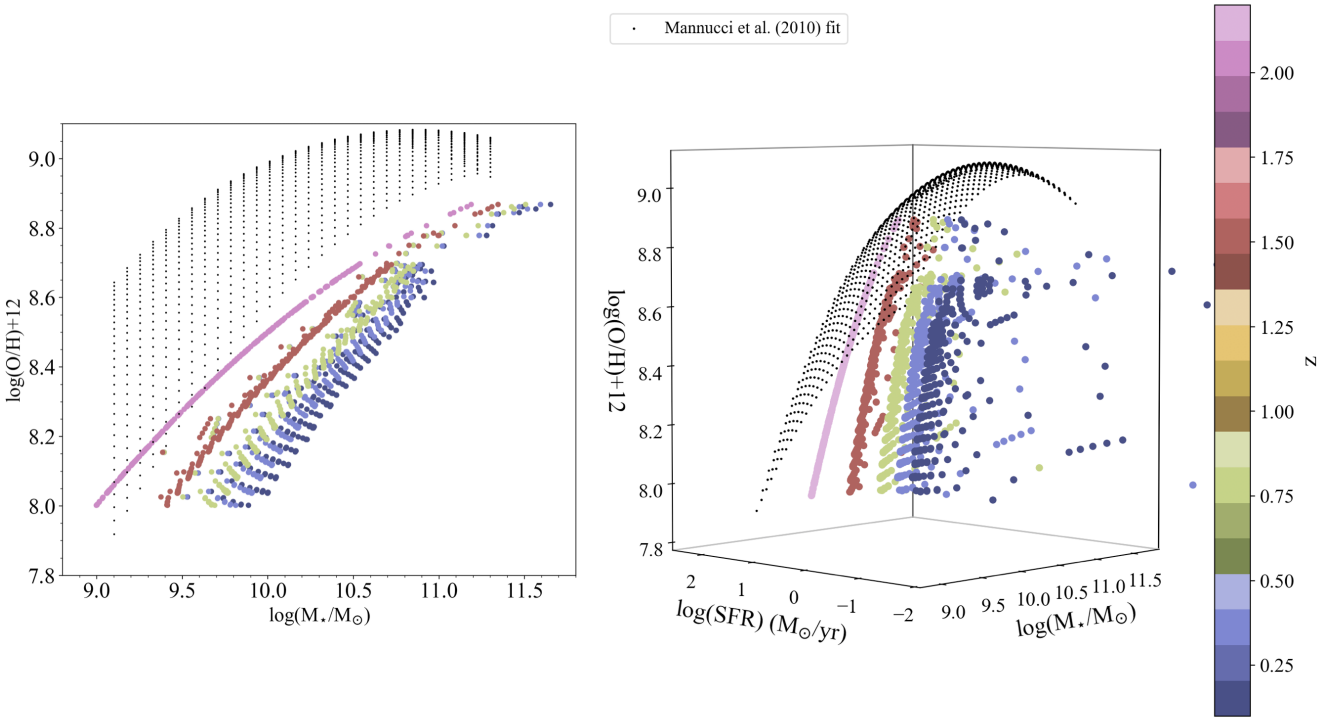

Fig. 18. As in Fig. 11 but for galaxies which at $z = 2.2$ follow the MZR of Maiolino et al. (2008) and the MSR derived by Pearson et al. (2018). The big solid circles are computed at redshifts $z = 2.2$, $z = 1.5$, $z = 0.8$, $z = 0.4$, and $z = 0.1$ and are colour-coded as a function of the redshift value. Black dots are as in Fig. 11.

at $z \sim 2.2$ a nearly flat MZR, set at the value of 12+log(O/H) $\sim$ 8.5 dex. It is worth mentioning that the computed metallicity of the NLR in the selected type 2 AGNs is based on calibrations from photoionization models of various rest-UV diagnostic line ratios. These methods are quite different from those adopted in "normal" star-forming galaxies as in Maiolino et al. (2008), which involve rest-optical lines and a combination of T_e-measurements and photoionisation modelling, hence the comparison between the two should be taken with caution.

As suggested by Mignoli et al. (2019), one of the possible reasons for a flat MZ relation is a selection effect in the sample. The high-ionization C IV emission line can cause culling of massive and dust-free hosts, not representative of the star-forming galaxy population at these redshifts. Another possibility is that the metallicity of the NLR is not a good proxy of that of the host galaxy, because an AGN can strongly affect not only the ionization properties of the gas, but also the circulation of metals in the ISM, e. g. by means of a strong outflow.

We make the hypothesis that the galaxy sample of Mignoli et al. (2019) include average star-forming galaxies. By means of our models, we have computed the forward evolution of the galaxies that at z=2.2 belong to the star-forming MSR of Pearson et al. (2018) and also present a flat MZR as observed by Mignoli et al. (2019), as shown in Fig. 19.

We have used the model with a constant SFE, fixed at the value of 1 Gyr^{-1} as discussed earlier.

From Fig. 19, we note that the required infall masses are larger than the galaxies that belong to the local MZR and the MSR (see Fig. 3).

A high oxygen abundance has to be already in place at high redshift even for galaxies with low stellar masses, and large infall masses are naturally accompanied by large metal production.
As for high stellar mass systems, the MSR imposes large SFR values ($1 < \log(\mathrm{SFR}/M_\odot, \mathrm{yr}^{-1}) < 2$). In order to maintain a high star formation level, large reservoirs of gas (i.e. large infall masses) are required.

In Fig. 19, we note that the mass-weighted ages versus stellar mass relation (computed ad different redshifts) shows a larger spread compared the one presented in Fig. 16 where at high redshift has been imposed the MZR of Maiolino et al. (2008). We tested that this difference is mainly due to the fact that in the last case galaxies with the same infalling mass present a similar SFH, and consequently they have the same mass-weighted age. In contrast, the high redshift flat MZR leads to a wide range of SFH at a fixed value for the infall mass in the successive evolution phases.

In their subsequent evolution, the galaxies settle onto an 'inverted' MZR, as already visible at $z = 1$. This occurs because, owing to their large SFR values, the system with the largest stellar masses become soon passive, hence their metal content does not change significantly at later times.

Low-mass galaxies are characterised by lower SFR values and by an already high metallicity. Their low SFR values and their relatively large infall masses allow them to maintain their star formation activity and to keep producing new metals, with an unavoidable consequent increase of their metallicity. In this case, their winds are not sufficient to lead to a significant decrease of their metallicity and to have them settled on a 'normal' MZR at lower redshifts.

These results might indicate that either our hypothesis regarding that these galaxies are on the MSR is inadequate, or that one fundamental ingredient is missing in our models which causes a substantial redistribution of metals, such as the feedback of an AGN. At present, investigations are on going in order to constrain the SFR of these systems and to assess which region

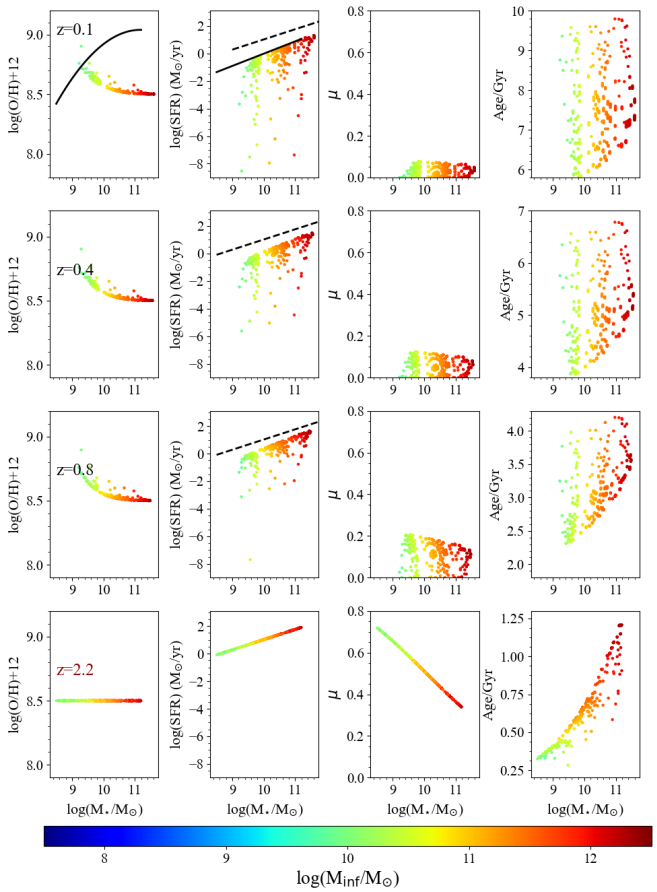

Fig. 19. Forward evolution from $z = 2.2$ to $z = 0.1$ of the galaxies which obey the analytical fit of the MZR at $z \sim 2.2$ observed by Mignoli et al. (2019) and the main sequence of star-forming galaxies as derived by Pearson et al. (2018). Starting from the left, in the first, second, third and fourth column the evolution of the MZR, SFR vs. stellar mass, gas fraction vs stellar mass and age-stellar mass relation are shown, computed at redshifts $z = 2.2$, $z = 0.8$, $z = 0.4$, and $z = 0.1$ (from bottom to top) The color coding stands for the infall gas mass value. The thick, black solid lines in the first two top-left panels are the MZR at redshift $z \sim 0.1$ of Kewley & Ellison (2008) and the MSR of Peng et al. (2010), respectively. The black dashed lines in each SFR-log($M_\star/M_\odot$) plot stand for the MSR derived in high redshift star forming galaxies by Pearson et al. (2018).

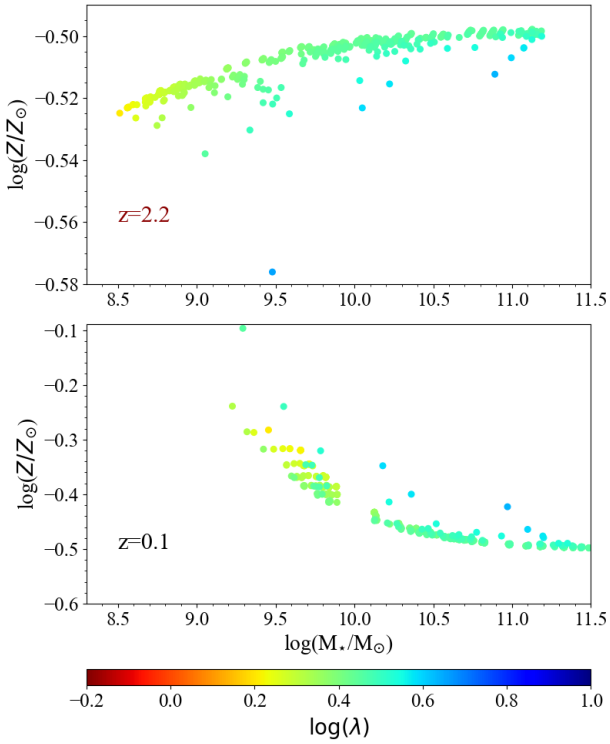

Fig. 20. Stellar mass-metallicity relation for the galaxies which follow the Mignoli et al. (2019) MZR and the high redshift star forming main sequence by Pearson et al. (2018) computed at redshift $z = 2.2$ (upper panel) and $z = 0.1$ (lower panel).

they occupy in the SFR-M_* diagram, to be compared to the MSR of 'normal' star forming galaxies observed at $z \sim 2$.

In Fig. 20 we explore the evolution of the stellar metallicity for the galaxies of the Mignoli et al. (2019) flat MZR. This quantity can be computed from our models in the following way:

$$\langle Z_\star(t) \rangle = \frac{\int_0^t dt'\, Z(t')\, \psi(t')}{\int_0^t dt'\, \psi(t')}. \quad (11)$$

Eq. 11 is by definition the mass-weighted stellar metallicity, i. e. the mass-weighted average of the metallicity of the stellar populations in each single galaxy (see Pagel 1997). It is interesting to note that at redshift $z = 2.2$, the shape of the stellar MZR is much different from the flat relation of the gas-phase metallicity. The stellar MZR presents more of a standard form, with an increasing behaviour at the low-mass edge and a flattening at $log(M_*/M_\odot) \sim 10$. This is a consequence of having imposed the MSR, and it is due to the fact that more massive objects have suffered on average stronger SF episodes at their earliest stages.

However, this relation is much flatter than the relations discussed previously in Sect. 5.2.1, as the variation between the metallicity of the lowest mass galaxies with $log(M_*/M_\odot) \sim 8.5$ and the plateau is of only 0.02 dex. At redshift $z = 0.1$, also the stellar metallicity presents an inverted shape, the with highest metallicity values at the lowest masses, as already seen in Fig. 19.

In summary, in our view the galaxies of a sample like the one of Fig. 19 and which build up a flat MZR do not represent an average sample of star-forming galaxies at high-redshift, which are expected to follow a steep MZR, as other works have shown (Erb et al. 2006; Maiolino et al. 2008). The sample of Fig. 19, in which all galaxies include a Type 2 AGN, is likely to be composed of systems at various evolutionary stages, and in which the AGN played an important role in regulating the star formation activity.

As a final note, another work in which the MZR in galaxies hosting type-2 AGN is the one of Matsuoka et al. (2018). Their sample includes high-z radio galaxies and X-ray selected radio-quiet AGNs at $1.2 < z < 4.0$ with stellar mass values $> 10^{10}\ M_\odot$. In this mass interval, Matsuoka et al. (2018) derive a MZR consistent with the one of Maiolino et al. (2008). However, due to the selection of their sample, their study does not probe the low-mass end of the MZR. In the future, metallicity measures of more extended datasets of AGN hosts will be needed to shed more light on the evolution of their MZR, and to further highlight possible differences with the scaling relations of star-forming galaxies.

6. Conclusions

In this paper we have studied the evolution of the systems which follow two fundamental observed scaling relations for star-forming galaxies, namely the MZR and the MSR. Our study was performed by means of the analytical, 'leaky-box' chemical evolution model of Spitoni et al. (2017b). In such model, galaxies are assumed to be formed by means of accretion of primordial gas, with an accretion rate which follows an exponential law, and in presence of galactic winds. In the model, each galaxy is characterized in terms of three model free parameters: the total infalling mass M_{inf}, the loading factor wind parameter λ and the the time-scale of gas accretion τ.

We focused on a given redshift, and we imposed that the galaxies must follow the observed MZR and the star-forming MSR measured at that particular redshift. First, we studied the properties of the local galaxies by imposing the MZR and the MSR observed at redshift $z = 0.1$, and analyzing their 'backward' evolution towards higher redshifts. On the other hand, by imposing the same scaling relations at higher redshift, we have computed a 'forward' evolution of the galaxies at lower redshifts and towards the present time.

Our main conclusions can be summarized as follows:

- By imposing the MZR and the MSR at redshift $z = 0.1$, we showed that the galaxies already present at redshift $z = 2.2$ are characterized by weak winds and long time scales of gas accretion. In fact, at low redshift these objects have to maintain a large reservoir of gas in order to be part of the local MSR and a high-metallicity, as they now build the high-metallicity plateau of the MZR. Moreover, the median of the infall time-scale distribution in two different bins of stellar masses ($M_\star < 10^{10} M_\odot$ and $M_\star > 10^{10} M_\odot$) decreases with decreasing redshift. This reflects that at each redshift, only the youngest galaxies can be assembled on the shortest timescales and still belong to the star-forming MSR. In the lowest mass bin, a decrease of the median τ is accompanied by an increase of the median λ value. This implies that systems which have formed at more recent times will need to eject a larger amount of mass to keep their metallicity at low values.
- Imposing both the MZR and the MSR naturally leads to an increasing relation between the mass-weighted age and the stellar mass which is qualitatively in agreement with the relation observed in local SF galaxies obtained with independent determinations. We note though that a quantitative agreement is difficult to assess because different observational estimates of the age-mass relation are sensitive to the assumption on SFH, SSP models and technique used. To our knowledge, such a direct connection between the MZR, MSR and downsizing was never shown before in any theoretical study. Moreover, no successful attempt has been performed so far to simultaneously reproduce these fundamental scaling relations within a cosmological framework, mostly because of an early overproduction of low-mass galaxies, which in such models nowadays are dominated by too old stellar populations (Calura et al. 2014, Somerville & Davé 2015).
- In a 3D space formed by SFR, oxygen abundances and stellar mass, the ancestors of the galaxies that follow the observed MZR and the star-forming MSR at $z = 0.1$ (as studied at $z \leq 2.2$) lie on a hyper-surface which is in good agreement with the fundamental metallicity relation of Mannucci et al. (2010).
- We studied the evolution of galaxies that at high redshift are part of both the observed MSR and of the MZR. By imposing at redshift $z = 2.2$ the MZR of Maiolino et al. (2008), we found that the large SFR values required by the high redshift MSR forces most of the galaxies to evolve passively at redshifts smaller than $z = 2.2$. In fact, the most massive objects show high stellar masses (built up in a short time) and high metallicity and must have consumed their reservoir of gas soon after leaving the MZR. Less massive galaxies, characterized by stronger winds, present a slower evolution, which manifests in a progressive steepening of the MZR towards recent times. In order to present at the same time low metallicities and high SFR values, it is clear that galaxies at $z = 2.2$ must have suffered much stronger stellar winds than galaxies belonging to the MZR and MSR at lower redshifts. Therefore, our findings confirmed that the observed MZRs and MSRs at different redshifts should not be interpreted as evolutionary sequences (see also Maiolino et al. 2008 and Lian et al. 2018a).
- In our analysis, we have calculated also the 'forward' evolution of high redshift objects which at $z \sim 2$ are characterized by a flat MZR, as observed by Mignoli et al. (2019). The sample by Mignoli et al. (2019) includes galaxies with a Type 2 AGN and selected from their C IV emission and for which the star formation rate is unknown. In this particular case, even low-mass galaxies have to present a high metallicity, already at early times. Also in this case, the system with the largest stellar masses become soon passive, whereas lower mass galaxies can still keep their star formation activity, with a further increase of their metallicity and despite their winds which, even if stronger than more massive systems, are not sufficient to deplete significantly their metal reservoirs. The implication is that, in their subsequent evolution, the galaxies settle onto an 'inverted' MZR. These results might indicate that one fundamental ingredient is missing in our model, which causes a substantial redistribution of metals within each single galaxy, such as the feedback of an AGN. Another possibility is that at present, these systems do not follow the MSR. At present, investigations are on going in order to constrain the SFR of these systems and to assess which region they occupy in the SFR-$M_\star$ diagram.

Acknowledgement

The authors thank the referee for the useful comments, which have certainly improved the paper. We thank G. Zamorani for useful suggestions. Funding for the Stellar Astrophysics Centre is provided by The Danish National Research Foundation (Grant agreement no.: DNRF106). E. Spitoni also acknowledges funding from the INAF-OAS visitor program. E. Spitoni and V. Silva Aguirre acknowledge support from the Independent Research Fund Denmark (Research grant 7027-00096B). V. Silva Aguirre acknowledges support from VILLUM FONDEN (Research Grant 10118). FC acknowledges support from grant PRIN MIUR 2017 - 20173ML3WW_001 and from the the INAF Main-Stream (1.05.01.86.31).

References

Boselli, A., Cortese, L., Boquien, M., et al. 2014, A&A, 564, A66
Brinchmann, J., Charlot, S., White, S. D. M., et al. 2004, MNRAS, 351, 1151
Bruzual, G. & Charlot, S. 2003, MNRAS, 344, 1000
Calura, F., Jimenez, R., Panter, B., Matteucci, F., & Heavens, A. F. 2008, ApJ, 682, 252
Calura, F. & Menci, N. 2009, MNRAS, 400, 1347
Calura, F., Menci, N., & Gallazzi, A. 2014, MNRAS, 440, 2066

Calura, F., Pipino, A., Chiappini, C., Matteucci, F., & Maiolino, R. 2009, A&A, 504, 373
Chabrier, G. 2003, PASP, 115, 763
Cowie, L. L., Songaila, A., Hu, E. M., & Cohen, J. G. 1996, AJ, 112, 839
Curti, M., Cresci, G., Mannucci, F., et al. 2017, MNRAS, 465, 1384
Curti, M., Mannucci, F., Cresci, G., & Maiolino, R. 2020, MNRAS, 491, 944
Elbaz, D., Daddi, E., Le Borgne, D., et al. 2007, A&A, 468, 33
Erb, D. K., Steidel, C. C., Shapley, A. E., et al. 2006, ApJ, 647, 128
Gallazzi, A., Brinchmann, J., Charlot, S., & White, S. D. M. 2008, MNRAS, 383, 1439
Gallazzi, A., Charlot, S., Brinchmann, J., White, S. D. M., & Tremonti, C. A. 2005, MNRAS, 362, 41
Geha, M., Blanton, M. R., Masjedi, M., & West, A. A. 2006, ApJ, 653, 240
Grisoni, V., Spitoni, E., & Matteucci, F. 2018, MNRAS, 481, 2570
Hirschmann, M., De Lucia, G., & Fontanot, F. 2016, MNRAS, 461, 1760
Iyer, K., Gawiser, E., Davé, R., et al. 2018, ApJ, 866, 120
Kannappan, S. J. 2004, ApJ, 611, L89
Kewley, L. J. & Dopita, M. A. 2002, ApJS, 142, 35
Kewley, L. J. & Ellison, S. L. 2008, ApJ, 681, 1183
Köppen, J., Weidner, C., & Kroupa, P. 2007, MNRAS, 375, 673
Larson, R. B. 1974, MNRAS, 169, 229
Lequeux, J., Peimbert, M., Rayo, J. F., Serrano, A., & Torres-Peimbert, S. 1979, A&A, 500, 145
Lian, J., Thomas, D., & Maraston, C. 2018a, MNRAS, 481, 4000
Lian, J., Thomas, D., Maraston, C., et al. 2018b, MNRAS, 474, 1143
Lian, J. H., Li, J. R., Yan, W., & Kong, X. 2015, MNRAS, 446, 1449
Madau, P. & Dickinson, M. 2014, ARA&A, 52, 415
Maiolino, R. & Mannucci, F. 2019, A&A Rev., 27, 3
Maiolino, R., Nagao, T., Grazian, A., et al. 2008, A&A, 488, 463
Mannucci, F., Cresci, G., Maiolino, R., Marconi, A., & Gnerucci, A. 2010, MNRAS, 408, 2115
Maraston, C. & Strömbäck, G. 2011, MNRAS, 418, 2785
Matsuoka, K., Nagao, T., Marconi, A., et al. 2018, A&A, 616, L4
Matteucci, F. 1994, A&A, 288, 57
Matteucci, F. 2012, Chemical Evolution of Galaxies
Mignoli, M., Feltre, A., Bongiorno, A., et al. 2019, A&A, 626, A9
Mortlock, A., Conselice, C. J., Bluck, A. F. L., et al. 2011a, MNRAS, 413, 2845
Mortlock, A., Conselice, C. J., Bluck, A. F. L., et al. 2011b, MNRAS, 413, 2845
Noeske, K. G., Weiner, B. J., Faber, S. M., et al. 2007, ApJ, 660, L43
Pagel, B. E. J. 1997, Nucleosynthesis and Chemical Evolution of Galaxies
Pasquali, A., Smith, R., Gallazzi, A., et al. 2019, MNRAS, 484, 1702
Pearson, W. J., Wang, L., Hurley, P. D., et al. 2018, A&A, 615, A146
Peng, Y., Maiolino, R., & Cochrane, R. 2015, Nature, 521, 192
Peng, Y.-j., Lilly, S. J., Kovač, K., et al. 2010, ApJ, 721, 193
Pérez-Montero, E., Contini, T., Lamareille, F., et al. 2013, A&A, 549, A25
Pipino, A. & Matteucci, F. 2011, A&A, 530, A98
Recchi, S., Spitoni, E., Matteucci, F., & Lanfranchi, G. A. 2008, A&A, 489, 555
Romano, D., Karakas, A. I., Tosi, M., & Matteucci, F. 2010, A&A, 522, A32
Salpeter, E. E. 1955, ApJ, 121, 161
Santini, P., Fontana, A., Castellano, M., et al. 2017, ApJ, 847, 76
Savaglio, S., Glazebrook, K., Le Borgne, D., et al. 2005, in American Institute of Physics Conference Series, Vol. 761, The Spectral Energy Distributions of Gas-Rich Galaxies: Confronting Models with Data, ed. C. C. Popescu & R. J. Tuffs, 425–428
Schmidt, M. 1959, ApJ, 129, 243
Somerville, R. S. & Davé, R. 2015, ARA&A, 53, 51
Spitoni, E. 2015, MNRAS, 451, 1090
Spitoni, E., Calura, F., Matteucci, F., & Recchi, S. 2010, A&A, 514, A73
Spitoni, E., Cescutti, G., Minchev, I., et al. 2019a, A&A, 628, A38
Spitoni, E., Gioannini, L., & Matteucci, F. 2017a, A&A, 605, A38
Spitoni, E., Silva Aguirre, V., Matteucci, F., Calura, F., & Grisoni, V. 2019b, A&A, 623, A60
Spitoni, E., Verma, K., Silva Aguirre, V., & Calura, F. 2020, A&A, 635, A58
Spitoni, E., Vincenzo, F., & Matteucci, F. 2017b, A&A, 599, A6
Spitoni, E., Vincenzo, F., Matteucci, F., & Romano, D. 2016, MNRAS, 458, 2541
Spolaor, M., Kobayashi, C., Forbes, D. A., Couch, W. J., & Hau, G. K. T. 2010, MNRAS, 408, 272
Tremonti, C. A., Heckman, T. M., Kauffmann, G., et al. 2004, ApJ, 613, 898
Trussler, J., Maiolino, R., Maraston, C., et al. 2020, MNRAS, 491, 5406
Vincenzo, F., Matteucci, F., Belfiore, F., & Maiolino, R. 2016, MNRAS, 455, 4183
Vincenzo, F., Spitoni, E., Calura, F., et al. 2019, MNRAS, L74
Weinberg, D. H. 2017, ApJ, 851, 25
Yuan, T. T., Kewley, L. J., & Richard, J. 2013, ApJ, 763, 9
Zahid, H. J., Dima, G. I., Kudritzki, R.-P., et al. 2014, ApJ, 791, 130

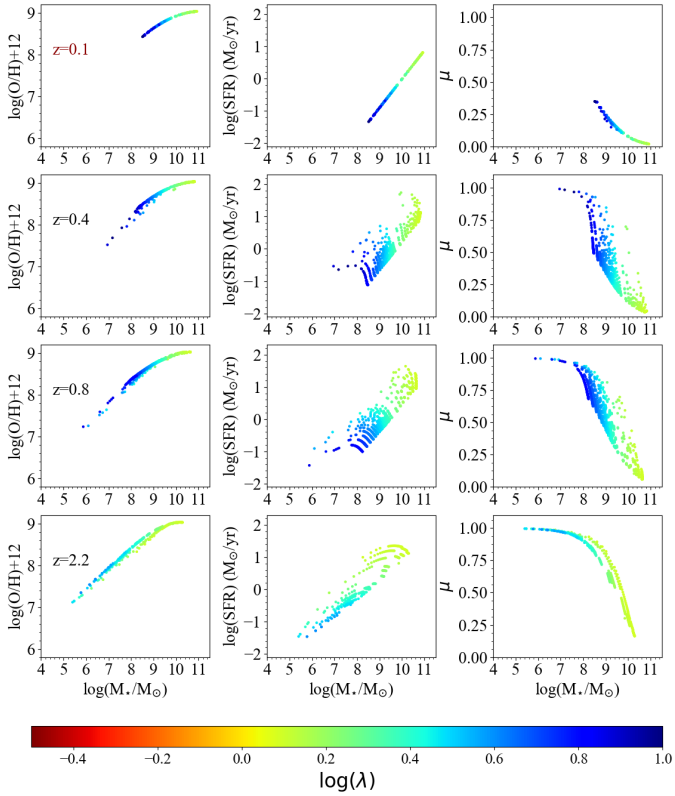

Fig. A.1. Backward evolution from $z = 0.1$ to $z = 2.2$ of the galaxies which obey the analytical fit of the observed MZR at $z \sim 0.1$ and the local main sequence of star-forming galaxies as in Fig. 2, but computed assuming a Chabrier (2003) IMF. In the first, second and third column we show the evolution of MZR, SFR vs stellar mass and gas fraction vs stellar mass, respectively. The colour coding indicates the loading factor parameter λ.

Appendix A: Model results with the Chabrier (2003) IMF

In this Appendix we present our model results similar to what discussed in Section 5.1.1 but computed assuming a Chabrier (2003) IMF. We still consider as constraints the observed MZR and star-forming main sequence at redshift $z = 0.1$, and we present the 'backward' evolution of some of the properties that build these two relations, including the gas fraction and age-mass relation.

As mentioned in Section 2 , the Chabrier (2003) IMF is richer in massive stars than the Salpeter IMF. If we assume the compilation of stellar yields presented by Romano et al. (2010), the oxygen yield per stellar generation computed with a Chabrier (2003) IMF is by a factor of ~ 2.3 larger than the value computed with the Salpeter (1955) IMF.

In Fig. A.1 we show the backward evolution of the MZR (first column), SFR-mass relation and gas fraction vs stellar mass relation for galaxies which at redshift $z = 0.1$ lie on the MZR and on the main sequence.

Compared to Salpeter (1955) case, in Fig. A.1 we note that the sequence of the first galaxies which have appeared at redshift $z = 0.8$ is more populated and more extended towards low stellar mass values. This is an obvious consequence of the higher yield for stellar generation, which leads to a more efficient chemical enrichment in all galaxies, and hence at any time galaxies with a smaller stellar mass can show the same oxygen abundance. Moreover, in Fig. A.2 we see that the Chabrier (2003) IMF requires stronger winds compared to the Salpeter (1955) as reported in Fig. 4, confirming previous results by Spitoni et al. (2017b).

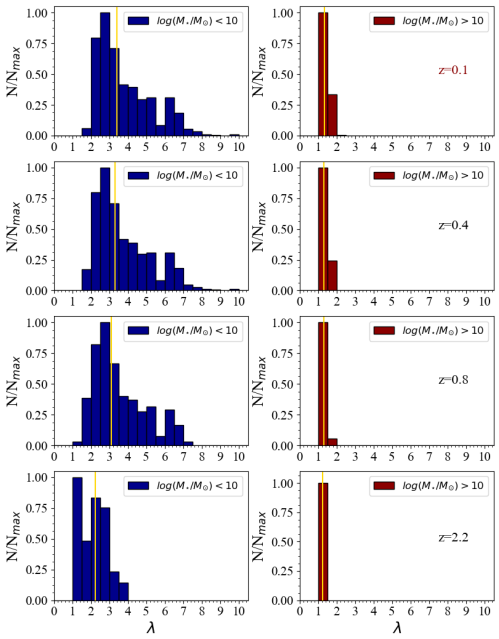

Fig. A.2. Distribution of the loading factor parameter λ for the galaxies of Fig. A.1 computed at redshifts $z = 2.2$, $z = 0.8$, $z = 0.4$, and $z = 0.1$ for 2 different bins of stellar mass (left: $log(M_\star/M_\odot) < 10$; right: $log(M_\star/M_\odot) > 10$). The yellow vertical lines indicate the median values of each distribution.

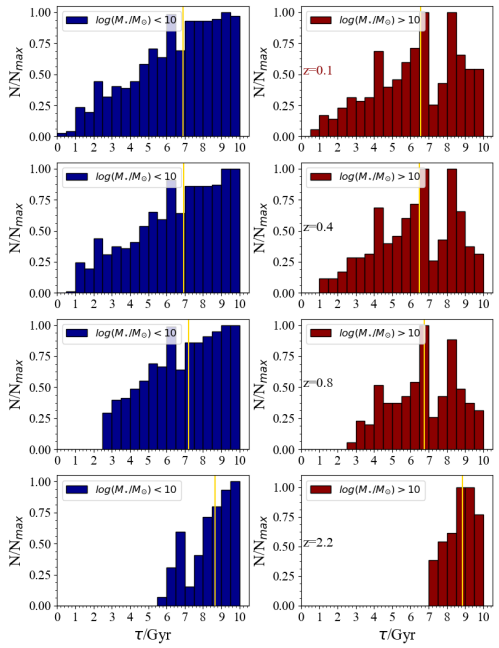

Fig. A.3. As in Fig. A.2, but in each panel the plotted distribution is for the infall time-scale parameter τ.

The evolution of the age-mass relation for our galaxies is shown in Fig. A.4 and the predicted age distribution computed at redshift $z = 0.1$ in two different redshift bins is shown in Fig. A.5. Both figures show that on average, the Chabrier (2003) IMF produces older galaxies than the Salpeter (1955) IMF.

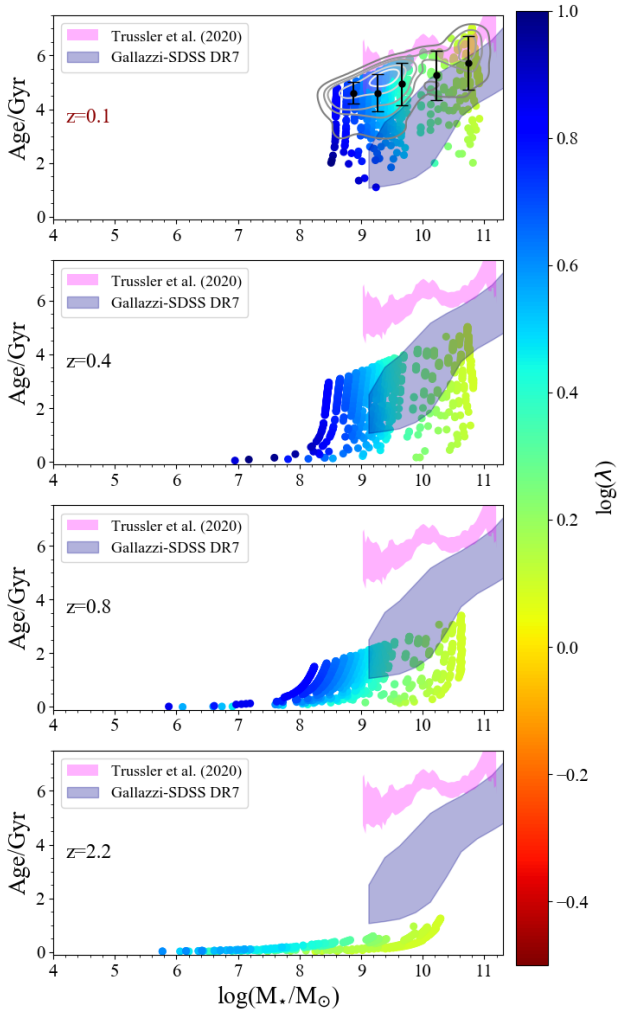

Fig. A.4. Backward evolution of the mass-weighted age versus stellar mass relation for the galaxies of Fig. A.1, computed adopting a Chabrier (2003) IMF.

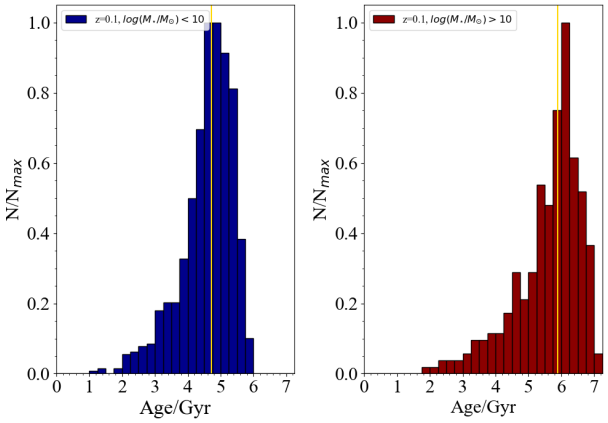

Fig. A.5. Age distribution for star-forming galaxies which are on the MZR at $z = 0.1$ in two different mass bins as in Fig. 7, computed assuming a Chabrier (2003) IMF.

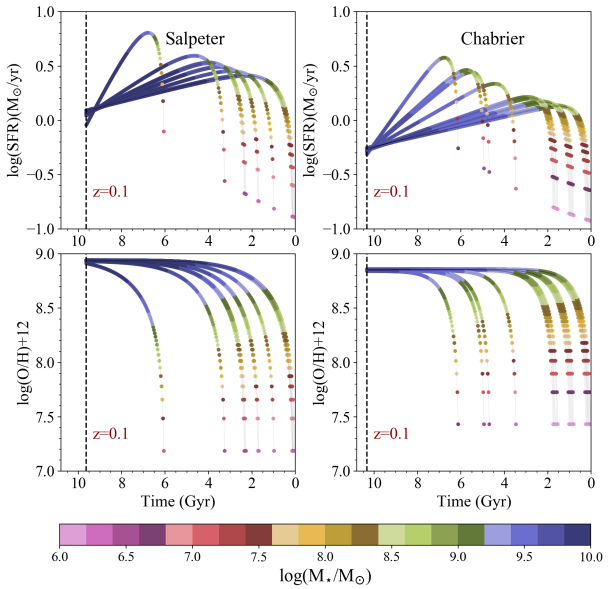

Fig. A.6. Evolution of star formation rate (upper panels) and oxygen abundance (lower panels) as a function of time for the galaxies with infall mass $M_{inf} = 10^{10.5} M_{\odot}$) which lie on the MZR of Kewley & Ellison (2008) and on the MSR as derived by Peng et al. (2010), computed assuming a Salpeter (1955) IMF (left panels) and a Chabrier (2003) IMF (right panels). The colour coding stands for the stellar mass.

This result seems to be in contrast with the ones obtained of Spitoni et al. (2017b) in which, by using as constraint for star-forming galaxies only the local MZR, the Chabrier (2003) IMF produced younger galaxies than the Salpeter (1955) IMF. This tension is only due to the fact that in this case we use also the MSR as further observational constraint for local star-forming systems.

In Fig. A.6 we compare the temporal evolution of the oxygen gas-phase abundances and of the SFR computed with two different IMFs. These quantities have been computed for a set of model galaxies which locally lie on both the MZR and on the MSR and which are characterised by a constant infall mass, fixed at the value of $M_{inf} = 10^{10.5}$ M$_{\odot}$

As expected, the metallicity of the galaxies with a Chabrier (2003) IMF reach their saturation value at earlier times than with the Salpeter (1955) IMF. Stronger winds are required to avoid an excessive increase of their metallicity, with the consequence of a significant removal of the gas available for star formation. This implies that, given the same infall mass, galaxies with a Chabrier (2003) IMF will be forced to evolve at a lower star formation regime.

With Chabrier (2003) IMF metallicity grows faster but stellar mass grows at a slower pace than with a Salpeter (1955) IMF. In the models shown in Fig. A.6 the SFH is continuous and, because of a more efficient gas removal in the case of the Chabrier (2003) IMF, the only way to have at the present day comparable stellar masses will be by means of a more extended SFH.
It is worth noting that in the case of Fig. A.6, the models with a Chabrier (2003) IMF will have smaller stellar masses than the ones with a Salpeter IMF. However, the same considerations will hold also for galaxies with the same present-day stellar masses which, in the case of a Chabrier (2003) IMF, will need to have started forming stars at earlier epochs, and which will thus present on average older mass-weighted ages. With reference to the galaxies drawn in Fig. A.6 using the Salpeter (1955) IMF, the average values for the stellar mass, the temporal evolution t_n computed at redshift $z = 0.1$ and the associated mass-weighted age Age(t_n) are respectively: $\log(M_{\star}/M_{\odot}) = 10.09$, $t_n = 8.15$ Gyr and Age(t_n) = 4.45 Gyr. On the other hand, with

the Chabrier (2003) IMF, we have that $\log(M_\star/M_\odot) = 9.71$, $t_n = 8.90$ Gyr and $\mathrm{Age}(t_n) = 5.11$ Gyr. Therefore, on average the model with the Chabrier (2003) IMF predicts older objects and with a smaller stellar mass content.